

Sadegh Imani Yengejeh
Seyedeh Alieh Kazemi
Andreas Öchsner

A Primer on the Geometry of Carbon Nanotubes and Their Modifications



Springer

SpringerBriefs in Applied Sciences and Technology

Computational Mechanics

Series editors

Holm Altenbach, Magdeburg, Germany

Lucas F.M. da Silva, Porto, Portugal

Andreas Öchsner, Southport, Australia

More information about this series at <http://www.springer.com/series/8886>

Sadegh Imani Yengejeh · Seyedeh Alieh Kazemi
Andreas Öchsner

A Primer on the Geometry of Carbon Nanotubes and Their Modifications



Springer

Sadegh Imani Yengejeh
Department of Solid Mechanics
and Design
Universiti Teknologi Malaysia (UTM)
Skudai
Malaysia

Andreas Öchsner
School of Engineering
Griffith University
Southport, QLD
Australia

Seyedeh Alieh Kazemi
Department of Mechanical Engineering
The University of Birjand
Birjand
Iran

ISSN 2191-530X ISSN 2191-5318 (electronic)
SpringerBriefs in Applied Sciences and Technology
ISSN 2191-5342 ISSN 2191-5350 (electronic)
SpringerBriefs in Computational Mechanics
ISBN 978-3-319-14985-1 ISBN 978-3-319-14986-8 (eBook)
DOI 10.1007/978-3-319-14986-8

Library of Congress Control Number: 2014959851

Springer Cham Heidelberg New York Dordrecht London
© The Author(s) 2015

This work is subject to copyright. All rights are reserved by the Publisher, whether the whole or part of the material is concerned, specifically the rights of translation, reprinting, reuse of illustrations, recitation, broadcasting, reproduction on microfilms or in any other physical way, and transmission or information storage and retrieval, electronic adaptation, computer software, or by similar or dissimilar methodology now known or hereafter developed.

The use of general descriptive names, registered names, trademarks, service marks, etc. in this publication does not imply, even in the absence of a specific statement, that such names are exempt from the relevant protective laws and regulations and therefore free for general use.

The publisher, the authors and the editors are safe to assume that the advice and information in this book are believed to be true and accurate at the date of publication. Neither the publisher nor the authors or the editors give a warranty, express or implied, with respect to the material contained herein or for any errors or omissions that may have been made.

Printed on acid-free paper

Springer International Publishing AG Switzerland is part of Springer Science+Business Media
(www.springer.com)

Preface

The main objective of this booklet is to provide a comprehensive categorization of carbon nanotubes and their modifications in terms of representative illustrations consisting of nanosheets, nanotubes, and their microscopic and atomic modifications. It is reported that the mechanical and physical properties of carbon nanostructures can be investigated with several computational and analytical approaches in a way that researchers can readily understand and accurately apply these findings in their own investigations. Through our research for this guide, we introduced the characterizations of carbon nanotubes and their modifications by making appropriate figures, which made our work a proper reference for addressing the configuration of these nanoparticles. This booklet is written to represent how these carbon nanostructures are constructed. In addition, the material and geometric properties of these nano-configurations have been addressed. Finally, some common software packages for geometry generation as well as several commercial finite element programs are introduced.

Sadegh Imani Yengejeh
Seyedeh Alieh Kazemi
Andreas Öchsner

Contents

1	Introduction	1
2	Literature Review	3
2.1	Axial Stiffness	3
2.2	Torsional Stiffness	7
2.3	Buckling Behavior	9
2.4	Vibrational Behavior	12
3	Geometric Definitions	17
4	Double and Multi-walled CNTs	25
5	Defective CNT Structures	29
5.1	Macroscopic Modifications	29
5.1.1	Straight Hetero-Junctions	29
5.1.2	Kink Hetero-Junctions	32
5.1.3	Three-Nanotube Junctions	38
5.1.4	Curvature	39
5.1.5	Twisting	40
5.1.6	Spiral Deformation	41
5.2	Atomic Modifications	45
5.2.1	Doping	45
5.2.2	Carbon Vacancies	45
5.2.3	Perturbation	47
6	Degenerated Tubes	49
6.1	Carbon Nanocone Structures	49
6.2	Buckminsterfullerene	50
6.3	Capped CNTs	51

7 Finite Element Modeling	53
7.1 Material and Geometric Properties.	53
7.2 Geometry Generation	53
8 Software Tools and Packages for Geometry Generation	59
8.1 CoNTub	59
8.2 Carbon/Boron Nitride Nanostructure Builder Plugin.	59
8.3 Nanotube Modeler	61
8.4 TubeGen	61
8.5 Ascalaph Designer	62
8.6 Atomistix ToolKit.	62
8.7 Materials Studio	63
8.8 Scigress.	65
References	67

Symbols and Abbreviations

a_1	Unit vector
a_2	Unit vector
b	Length of C–C bond
C_h	Chiral vector
d	Diameter of CNT
\bar{d}	Average diameter
d_{wide}	Diameters of the wider tubes
d_{thin}	Diameters of the thinner tubes
E	Young's modulus
G	Shear modulus
I	Second moment of area
l_{thin}	Length of the thinner tube
$l_{\text{connecting}}$	Length of the connection region
l_{wide}	Length of the thinner tube
n	Integer
m	Integer
R_b	Bond radius
Δr	Change in the distance between two atoms
θ	Chiral angle
η	Aspect ratio of the junction
CNT	Carbon nanotube
DWCNT	Double-walled carbon nanotube
FEA	Finite element analysis
FEM	Finite element method
IMJ	Intramolecular junction
MD	Molecular dynamics
MWCNT	Multi-walled carbon nanotube
SWCNT	Single-walled carbon nanotube
SEM	Scanning electron microscopy
TEM	Transmission electron microscopy

Chapter 1

Introduction

Carbon nanotubes (CNTs) are hollow cylinders, built by hexagonal unit cells, shaped by carbon atoms which were found by Iijima in 1991 [1], where he reported the preparation of a new type of finite carbon structure consisting of needle-like tubes. In carbon nanotube history, single-walled CNTs (SWCNTs) should be distinguished from multi-walled CNTs (MWCNTs). It is perfectly clear that the formation of SWCNTs was first reported in [2, 3]. The work on MWCNTs was boosted by the report made by Iijima in 1991 [1] on their occurrence in the hard deposit growing at the cathode during electric arc experiments to produce fullerene. Since their discovery, these nanostructures have attracted worldwide attention; numerous opportunities and possibilities have been opened to create a new generation of materials and structures that possesses unique physical properties [4]. The study of CNTs is one of the most promising domains in the area of physics, mechanics, chemistry, and material science [5]. Transmission electron microscopy (TEM) and scanning electron microscope (SEM) images of MWCNTs are shown in the following Figs. 1.1 and 1.2.

A wide range of applications of CNTs have been reported in the literature, including applications in nanoelectronics, nanodevices, and nanocomposites [1, 4, 5].

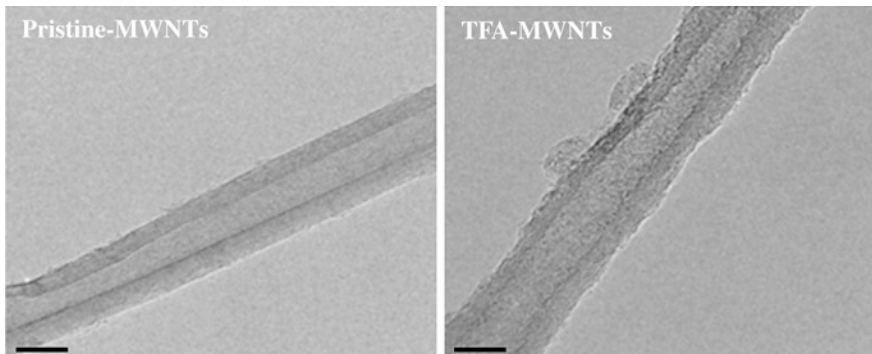


Fig. 1.1 TEM images of pristine and functionalized MWCNTs [6]

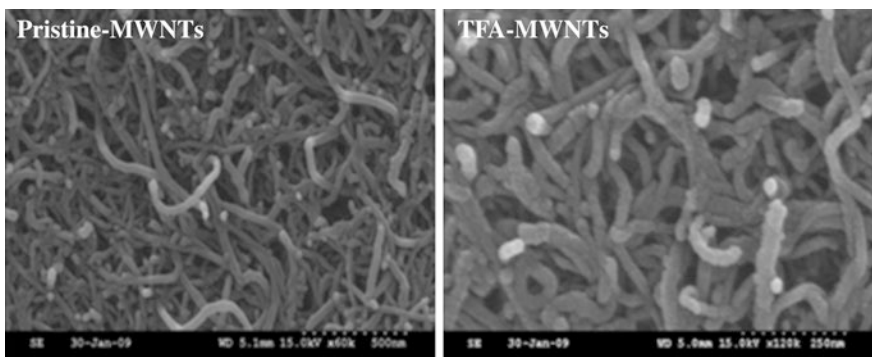


Fig. 1.2 SEM images of pristine and functionalized MWCNTs [6]

Chapter 2

Literature Review

2.1 Axial Stiffness

The stiffness of an object is the rigidity of it in response to an applied load, as shown schematically in Fig. 2.1. The original length L is increased to $L + \Delta L$ under the influence of the external force F .

By applying Hooke's law, the Young's modulus of the CNTs can be calculated by the following equations:

$$\sigma = \text{stress} = F/A \quad (2.1)$$

$$\varepsilon = \text{strain} = \Delta L/L \quad (2.2)$$

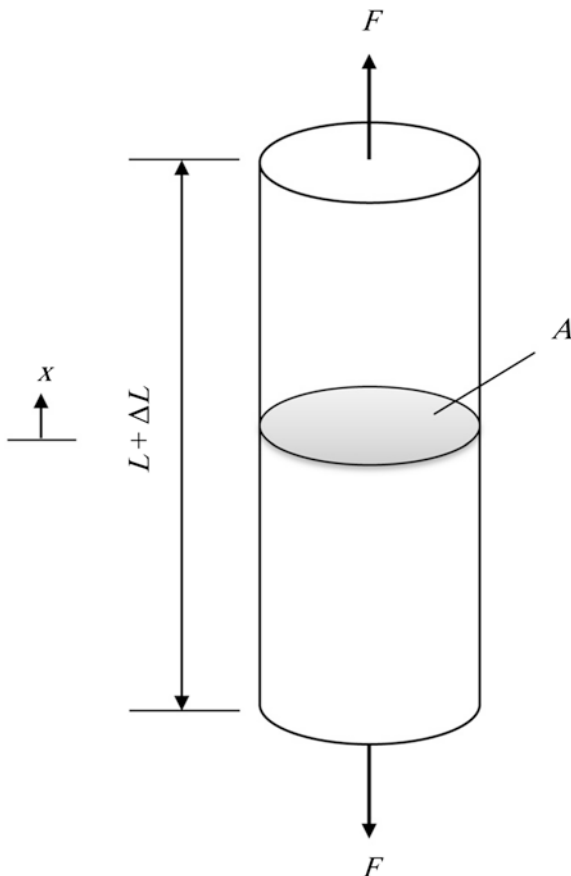
$$E = \text{Young's modulus} = \sigma/\varepsilon \quad (2.3)$$

The following paragraph presents the results of several investigations on the evaluation of CNTs tensile properties.

Natsuki et al. [7] developed an analytical method for modeling the elastic properties of SWCNTs based on a link between molecular and solid mechanics. In their investigation, a SWCNT is regarded as a continuum-shell structure which is compared to the discrete molecular configuration linked by the C–C bond. They studied the elastic properties of SWCNTs as a function of the nanotube size. Liew et al. [8] examined the elastic and plastic properties of CNTs under axial tension applying the molecular dynamics (MD) approach. They obtained the stress-strain responses to describe the elastic and plastic behavior of single and multi-walled CNTs in their investigations. Moreover, they took the brittle fracture under consideration due to the bond breaking. Consequently, their MD simulations revealed the fact that the outermost layer is the main spot of the fracture damage of CNTs. Later in 2006, Meo and Rossi [9] proposed a finite element (FE) model, based on the molecular dynamics theory so that they would investigate the fracture progress in armchair and zigzag CNTs with defects under uniaxial tensile stress. Their examinations revealed the complete load-displacement relationships for a (5,5) and a (9,0) CNT up to the complete fracture. Based on their findings, they

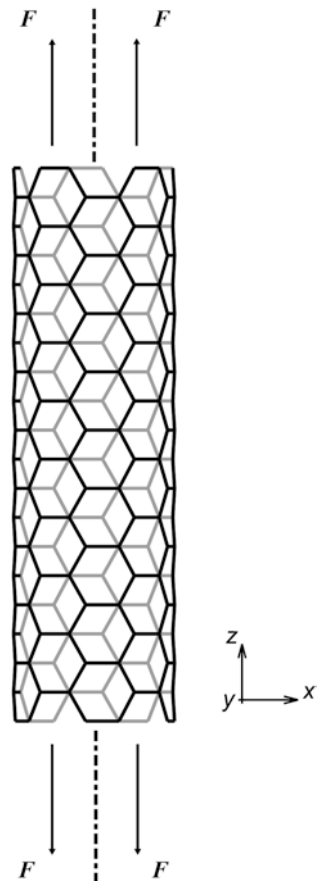
concluded that the effect of chirality on the mechanical properties and failure mode of CNTs was quite significant. A year later, Tserpes and Papanikos [10] examined the effect of Stone-Wales defects on the tensile behavior and fracture of different types of SWCNTs, using an atomistic-based progressive fracture model. They predicted a particular reduction in failure stress and failure strain in armchair SWCNTs, contrary to zigzag ones; ranging from 18 to 41 %, respectively. Afterwards, Xiao et al. [11] conducted a computational study on the investigation of the tensile behavior of SWCNTs, using a self developed nano-mechanical testing device. They also studied the tensile strength of SWCNT bundles. They concluded that the tensile strength distribution of CNTs can be adequately described by a two-parameter Weibull model. They finally proposed a method in order to determine the tensile strength distribution of individual CNTs. In 2009, Kuang and He [12] conducted a study to investigate the effect of chemical functionalization on the axial Young's moduli of SWCNTs based on molecular mechanics simulation. They concluded that the Young's moduli depend strongly on the chirality of the CNTs. In addition, molecular mechanics revealed that the functionalization

Fig. 2.1 A simple schematic illustration of a tensile test to determine the material stiffness



of SWCNTs results in a decrease of the Young's moduli of the corresponding SWCNT composites. Later in 2011, Mohammadpour and Awang [13] developed a FE model based on the molecular mechanics approach for evaluating the tensile properties of SWCNTs. In their investigation, individual CNTs were simulated as a frame-like configuration and the primary bonds between two nearest-neighbor atoms were treated as beam elements. A computational simulation for investigating the mechanical properties of CNTs was conducted by Lu and Hu [14] in 2012. They developed an improved 3D FE model for different types of CNTs. They also investigated the elastic stiffness of graphene as well as the effect of diameters and helicity on the Young's modulus and shear modulus of SWCNTs. Ghavamian et al. [15] investigated the mechanical properties of single- and multi-walled CNTs in their perfect and imperfect form. They introduced some types of imperfections in different amounts to the perfect models. Finally the elastic behavior of the defected CNTs was obtained and compared with those of perfect ones. Their findings indicated that the existence of any kind of imperfection in the perfect models leads to lower stiffness values. Recently in 2013, Kinoshita et al. [16]

Fig. 2.2 (5,5)-armchair CNT under tensile test



proposed a study in order to investigate the mechanical properties of SWCNTs with one-dimensional intramolecular junctions (IMJs), using first-principle density functional theory calculations. In addition, they examined the effects of pentagon-heptagon defects at a junction on the tensile strength, Young's modulus and breaking strain of CNT-IMJs. The average value of the Young's modulus of CNTs was around 0.9 TPa. They finally found that the tensile strength and breaking strain of CNT-IMJs depend on the position of pentagon-heptagon defects. Figure 2.2 shows a simulated model of a CNT under tensile test.

Figure 2.3 compares the average stiffness of a CNT with other classical engineering materials. The average values for the classical engineering materials were taken from [17–19].

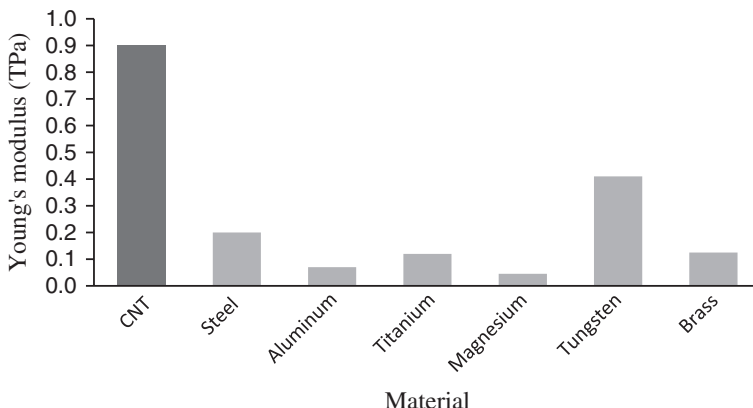


Fig. 2.3 Average Young's modulus values of some classical engineering materials

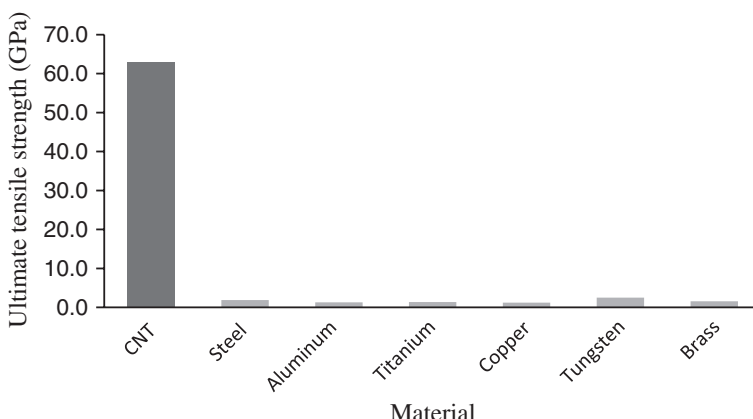


Fig. 2.4 Average ultimate tensile strength values of some classical engineering materials

It can be seen from this figure that the stiffness of a CNT is much higher than that of classical engineering materials, for instance more than four times higher than steel's. The average ultimate tensile strength of a CNT and other classical engineering materials is shown in Fig. 2.4. These average values were taken from [17–19].

As shown in the diagram above, the ultimate tensile strength of CNTs is approximately 70 times larger than steel.

2.2 Torsional Stiffness

In a torsion test, a specimen is twisted by introducing an arbitrary angular rotation θ around their major axis and consequently, the corresponding reaction torque is obtained. Figure 2.5 shows a schematic illustration of a torsion test on a simple cylinder.

For the evaluation of such a torsion test, the shear modulus of the material can be calculated by the following equation [20]:

$$G = TL/\theta J \quad (2.4)$$

where θ , T , L and J represent the twisting angle, the torque, the length and the polar moment of inertia, respectively.

The investigation on the torsional stiffness of CNTs is very important for which several studies are presented in the following.

In 2003, Li and Chou [21] investigated the torsional stiffness of MWCNTs. They assumed that the nested individual layers of a MWCNT act as single-walled frame-like structures and simulated by the molecular structured mechanics methods. Their results indicated that the shear moduli and Young's moduli of MWCNTs are in the ranges of 0.4 ± 0.05 and 1.05 ± 0.05 TPa, respectively. In addition, they concluded that the tube diameter, chirality and number of

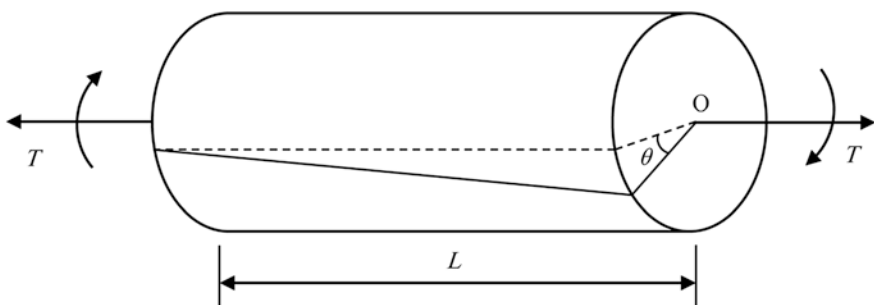
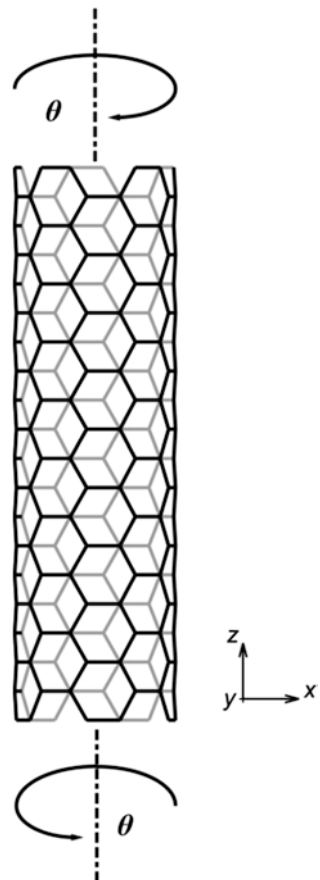


Fig. 2.5 A simple schematic illustration of a torsion test to determine the shear modulus

tube layers have a major effect on the elastic properties of MWCNTs. They also conducted a structural mechanics method for modeling the deformation of CNTs [20]. Their investigations indicated that CNTs are geometrical frame-like structures and the primary bonds between two nearest neighboring atoms act like load bearing beam members. Based on their results, they concluded that by increasing the tube diameter, the Young's moduli of CNTs increase. Later in 2006, Kalamkarov et al. [22] investigated the behavior of CNTs applying different techniques. The first approach models CNTs as an inhomogeneous cylindrical network shell applying the asymptotic homogenization method. Their second approach was based on FE models. Such models were developed for CNTs with different numbers of layers. They could predict the elastic and shear moduli of the CNTs using the deformations from the FE simulations. In addition, they investigated the dependence of the mechanical properties on the number of nanotubes in multi-walled structures. The shear modulus was found to vary from 0.14 to 0.47 TPa for SWCNTs and 0.39–0.62 for double/multi-walled

Fig. 2.6 (5,5)-armchair CNT under torsion test



CNTs. After that, To [4] obtained the elastic properties of SWCNTs experimentally and computationally. He mainly investigated the Young's and shear moduli of SWCNTs. He pointed to the fact that the Young's and shear moduli of SWCNTs have been estimated to be constant within the linear domain. In their study, the classical theory of elasticity could be used for the determination of the Young's and shear moduli of SWCNTs. Tsuda et al. [23] evaluated the interface shear strength of CNT-dispersed polymer composites. They pull-out an individual MWCNT from a MWCNT-dispersed/PEEK composite applying a nano-pullout testing system. Moreover, they measured the tensile load using the elastic deformation of an AFM cantilever. In 2012, Viet and Kuo [24] employed both shear lag modeling and finite element analysis (FEA) to analyze the stress distribution in the graphene layers. They also investigated the effect of the aspect ratio on shear transfer efficiency. They evaluated the effective shear modulus of a fractured CNT with respect to the number of broken layers. Their findings revealed that the layered configuration can increase the shear stress concentration. Recently in 2013, Ghavamian et al. [25] obtained the shear modulus of SWCNTs and MWCNTs applying the finite element method (FEM). In order to clarify the most appropriate approach, they determined the shear modulus of CNTs by simulating two basic tests. First, they directly evaluated the modulus by applying a torsion test. Second, they simulated the tensile test in order to obtain the shear modulus. The comparison of both approaches indicates that CNTs behave rather as an anisotropic material. Figure 2.6 illustrates the simulated model of a CNT under torsion test.

2.3 Buckling Behavior

Buckling is understood as a structural instability which results in the sudden failure of a mechanical component. This instability is characterized by the loss of structural stiffness and is susceptible for slender and thin-walled structures as in the case of the considered CNTs. In the basic theory of elasticity, the critical buckling load of a straight elastic beam is presented by Eq. (2.5) as [26]:

$$P_{\text{cr}} = \frac{n^2 \pi^2 EI}{(KL)^2} \quad (2.5)$$

In the above equation, E is the Young's modulus of the material, n represents the buckling mode, K is the effective length constant and I is the structure's second moment of area. As the classical structure of CNTs is mostly presented by a hollow cylinder, Eq. (2.6) can be used to obtain analytical results for straight CNTs as:

$$I = \pi [(d + t)^4 - (d - t)^4]/64 \quad (2.6)$$

where t is the thickness of the tube's shell and d represents the diameter of the pertaining tube.

Figure 2.7 illustrates different possibilities of buckling tests and resultant critical loads that can be acquired theoretically.

The following paragraph summarizes several related studies where the buckling behavior of CNTs was investigated.

Wang et al. [28] conducted a computational study in order to simulate the compression deformation of SWCNTs, using the Tersoff-Brenner potential to depict the interactions of atoms in CNTs. They found that by increasing the radius of CNTs, the Young's modulus of the tubes decreases. In addition, they indicated that there are two different buckling modes for SWCNTs. Kang et al. [29] conducted a study to investigate the buckling behavior of intramolecular junctions (IMJs) under axial compression, using both MD and finite element (FE) analysis. According to their results, it was proven that the critical compressive strain is dependent on the length and radial dimensions of the IMJ. However, it is insensitive to the chirality of the IMJ. An investigation in the mechanical properties of the CNTs under various loading conditions, including compression, tension, torsion, bending and hydrostatic pressure was performed by Motevali et al. [30]. Their results indicated that the buckling deformations and the critical loads are highly dependent on the ratio of rotational and axial displacement rates. Moreover, they proposed a relationship between the normal and shear stresses which can be established for finding the stress limits when designing practical CNT-based systems in which combined load might be used. The main focus of Poelma et al. [31] in their research was mainly to investigate the buckling behavior of fixed-fixed, both SWCNTs and MWCNTs under axial compressive load, using analytical continuum theory and MD. In addition, in order to apply the boundary conditions

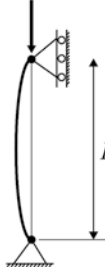
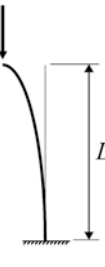
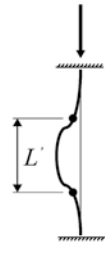
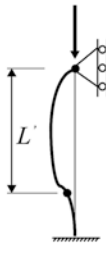
Pinned-pinned column	Fixed-free column	Fixed-fixed column	Fixed-pinned column
$P_{cr} = \frac{\pi^2 EI}{L^2}$	$P_{cr} = \frac{\pi^2 EI}{4L^2}$	$P_{cr} = \frac{4\pi^2 EI}{L^2}$	$P_{cr} = \frac{2.046\pi^2 EI}{L^2}$
			
$L' = L$	$L' = 2L$	$L' = 0.5L$	$L' = 0.699L$
$K = 1$	$K = 2$	$K = 0.5$	$K = 0.699$

Fig. 2.7 Different conditions of the buckling test, adopted from [27]

and extract the reaction forces during the MD simulation, they used an approach based on the tethering of atoms. The results of their simulation revealed the defects at the ends of the CNT. As a result, the influence of vacancy defects on the critical buckling load and strain was proven to be small at room temperature. Ansari and Rouhi [32] developed an atomistic FE model to study the buckling behavior of CNTs with different boundary conditions. Based to their model, they obtained and then compared the critical compressive forces of SWCNTs with different boundary conditions. They concluded that at low aspect ratios, the critical buckling load of nanotubes decreases considerably with increasing aspect ratio; while at higher aspect ratios, buckling load slightly decreases as the aspect ratio increases. Finally, they found out that increasing the aspect ratio at a given radius results in a convergence of buckling envelops associated with armchair and zigzag CNTs. Xin et al. [33] performed MD simulations for the axial compression of both perfect and defective SWCNTs. Based on their findings, it was proven that any change in length, the chirality, and the initial structural defects of the tube would be effective on the buckling and axially compressive properties of SWCNTs. The investigation on the dependence of the mechanical characteristics of SWCNTs on their length, radius, and chirality was conducted by Talukdar et al. [34]. Their findings revealed the fact that the tensile properties of zigzag and armchair CNTs are not dependent

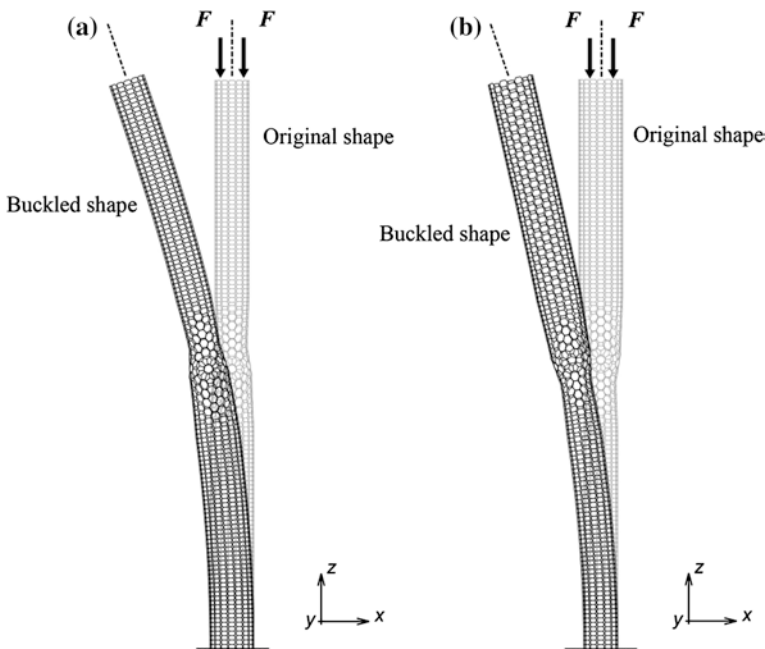
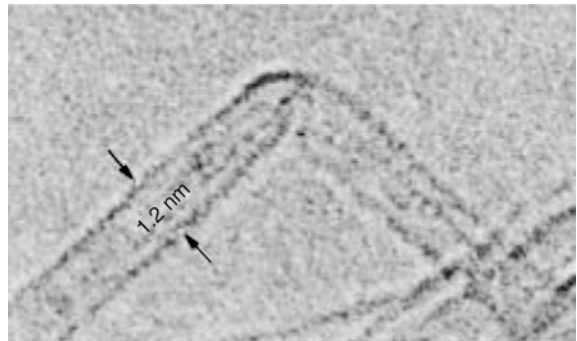


Fig. 2.8 (7,7)–(9,9)-straight hetero-junction CNT's first mode under buckling load in original and buckled form with two different types of cantilevered boundary conditions: **a** wider tube fixed, and **b** thinner tube fixed

Fig. 2.9 Experimental observation of the buckling behavior of a CNT at nanoscale dimensions [36]



on their length. The fracture patterns showed different modes in each case. In their model, buckling produced wavy structures, kinks, bending, and twisting. Chang et al. [35] obtained analytical solutions for the critical buckling strain of single-walled achiral CNTs under axial compression. They conducted their study based on a molecular mechanics model. According to their findings, it was revealed that zigzag tubes are more stable than armchair tubes with the same diameters. After comparing their results given by continuum mechanics models they found out that the continuum mechanics model underestimates the critical buckling strain for smaller tubes if a Young's modulus for larger tubes is adopted. Moreover, they concluded that the van der Waals interaction has little effect on the critical buckling strain for double-walled carbon nanotubes (DWNTs). The simulated models of hetero-junctions with original and buckled shape are shown in Fig. 2.8.

Figure 2.9 illustrates experimental observation of the buckling behavior of a CNT.

2.4 Vibrational Behavior

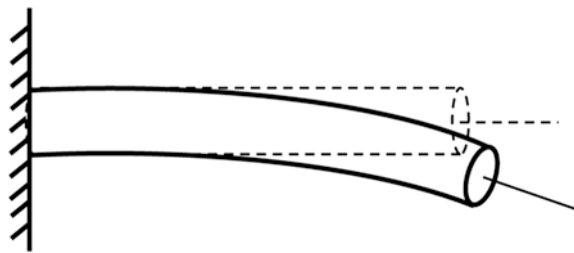
The natural frequency is the frequency of a vibrating system at which the system oscillates at greater amplitude because of the existence of the resonance phenomenon. Geometry, mass, and applied boundary conditions are the factors which influence these quantities. The natural frequency is mainly evaluated to examine the vibrational behavior of structural members. Figure 2.10 illustrates a simple schematic shape of the first mode of vibration of a beam.

The first natural frequency of an Euler-Bernoulli beam element under cantilevered boundary conditions is defined by the following equation [37]:

$$f = (3.5156/2\pi)\sqrt{EI/\bar{m}L^4} \quad (2.7)$$

where E , I , \bar{m} and L are the Young's modulus, the second moment of area, the mass per unit length and the length of the CNT, respectively. The results of several studies on the vibrational characteristics and buckling behavior of CNTs are presented.

Fig. 2.10 A simple schematic illustration of the first mode of vibration of a beam



Behera and Chakraverty [38] investigated the vibrational behavior of nonlocal nanobeams based on Euler-Bernoulli and Timoshenko beam theories. They established expressions for the free vibration of Euler-Bernoulli and Timoshenko nanobeams within the framework of Eringen's nonlocal elasticity theory. In their study, the numerical results for the free vibration of nanobeams have been presented, applying simple polynomial and orthonormal polynomials in the Rayleigh-Ritz method. In this way, one can easily handle the specified boundary conditions at the edges. They also compared their investigations with the results of the existing literature. Finally they could obtain frequency parameters for different scaling effect parameters and boundary conditions. Their results revealed that small scale effects considerably influence the free vibration of nanobeams. In addition, they concluded that nonlocal frequency parameters of nanobeams are smaller when compared to the corresponding local ones. Through nonlocal elasticity theory, the axial vibration of single-walled CNTs embedded in an elastic medium was investigated by Aydogdu [39]. He also used the nonlocal constitutive equations of Eringen in the formulations. He discussed the effect of various parameters such as stiffness of the elastic medium, boundary conditions, and parameters on the axial vibration of nanotubes. He finally concluded that the axial vibration frequencies of the embedded CNTs are highly overestimated by the classical continuum rod model which ignores the effect of small length scale. After simulating two configurations of homogeneous CNTs (armchair and zigzag) based on the FE method, Ghavamian and Öchsner [40] introduced the three most likely defects to their models in order to represent defective forms of SWCNTs. These defects are Si-doping, carbon vacancy, and perturbation. They finally investigated and compared the vibrational properties of perfect and defective CNTs. Their results showed that SWCNTs have a natural frequency in the range of 18.69 and 24.01 GHz. Furthermore, it was concluded that the existence of any type of irregularities on CNTs leads to a lower value of natural frequency and vibrational stability. Seyyed Fakhrabadi et al. [41] conducted a study investigating the vibrational properties of the two and three junctioned CNTs with different geometries and boundary conditions. They applied a well-known molecular mechanics approach to the modal analysis of the CNTs. Their results covered the natural frequencies and their corresponding mode shapes. They presented the results of the two junctioned CNTs with different lengths and diameters and also with cantilever from right side, left side, and doubly clamped boundary conditions in detail. In addition, they investigated the natural frequencies

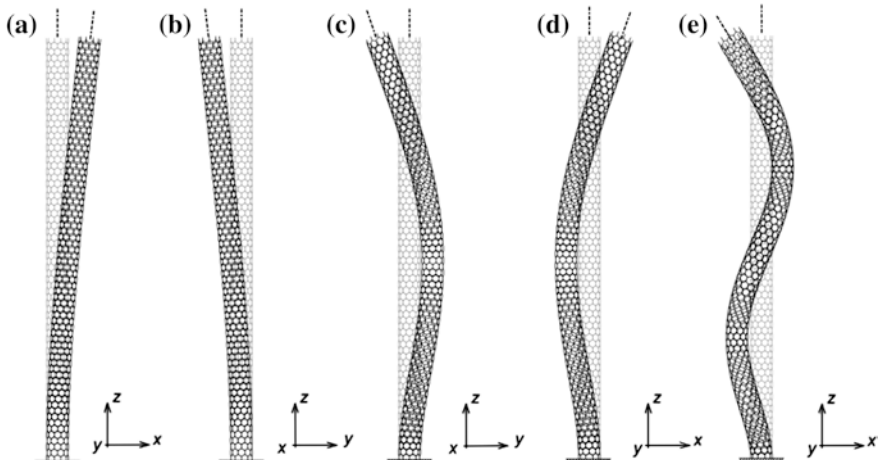


Fig. 2.11 First five eigenmodes of a (10,0)-zigzag CNT

of the three junctioned CNTs with different lengths, diameters, and various boundary conditions. Rahmandoust and Öchsner [27] simulated single-walled carbon nanotubes in their perfect forms applying the finite element method (FEM) in the MSC. Marc software. Afterwards, they investigated the buckling behavior and resonant frequency modes of zigzag and armchair models. Their results indicated that there were similarities between the buckling behaviors of SWCNTs under cantilevered boundary conditions. Nevertheless, it was observed that the value of the first mode of frequency is more accurate than the higher modes. Firouz-Abadi and Hosseiniyan [42] conducted a study to investigate the free vibrational characteristics of SWCNTs in the vicinity of a fully constructed graphene sheet. They applied a molecular structural mechanics model and considered nonlinear van der Waals interactions in order to obtain the elastic deformation of the nanotube. Their investigation results were in very good agreement with the results in the literature. Consequently, they carried out a survey on the natural frequency of the CNTs beam-like modes in various distances from the graphene sheet. Biao et al. [43] employed an atomic finite element model based on a virtual spring model for armchair and zigzag SWCNTs in order to determine the relation between axial load and frequency shift. They also introduced the Tersoff-Brenner potential so that the interaction between the atoms would be defined as well as the mechanical properties of the springs in the model. By applying finite element theory and techniques, they could obtain the fundamental frequency shifts of transverse and radial vibration modes of SWCNTs. They found out that the fundamental frequencies of the two modes are typically as high as hundreds of gigahertz. In addition, by increasing the stretching load, these frequencies decreased linearly, despite growing with the increase of the compression load. They studied various types of nanotubes with different diameters, chirality, and lengths. Their results revealed the fact that by increasing the length and diameter, both the frequency sensitivities

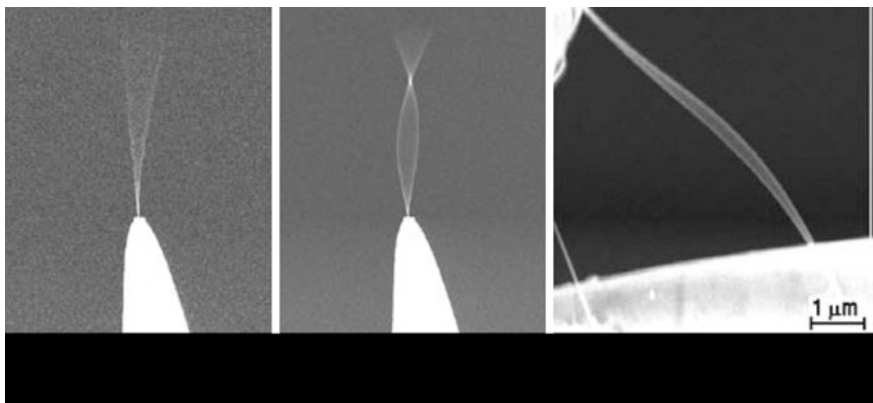


Fig. 2.12 SEM images showing the first harmonic and the second harmonic resonant oscillations of an individual MWCNT, and the resonant oscillation of a MWCNT bounded at both ends [45]

for transverse and radial vibration modes decrease. Nevertheless, they proved that there are some exceptions in nanotubes with small-diameter. Filiz and Aydogdu [44] investigated the axial vibration of CNTs hetero-junctions using a nonlocal rod theory. They applied the nonlocal constitutive equations of Eringen in the formulations. They used various types of hetero-junctions with different lengths, chirality, and diameters. For each case, the effect of nonlocality, length of the CNTs, and length of each segment were investigated. Their results showed that by joining CNTs good vibrational properties are obtained by suitable selection of parameters. Figure 2.11 illustrates the first five eigenmodes of a CNT in the simulation.

The SEM image of resonant oscillations of an individual MWCNT is shown in Fig. 2.12.

Chapter 3

Geometric Definitions

CNTs are assumed to be a hollow cylinder shaped configuration based on the major similarity between a CNT and the graphene atomic structure. Such a CNT can be imagined by rolling a graphene sheet into a cylinder with diameters ranging from 1 to 50 nm and lengths over 10 μm . The geometry of a CNT is defined by the chiral vector \mathbf{C}_h and the chiral angle θ . The chiral vector is represented by two unit vectors \mathbf{a}_1 and \mathbf{a}_2 and two integers m and n as it is shown by the following equation [46]:

$$\mathbf{C}_h = n\mathbf{a}_1 + m\mathbf{a}_2 \quad (3.1)$$

The basic configuration of CNTs can be defined based on the chiral vector or angle by which the sheet is rolled into a cylinder, as shown in Fig. 3.1.

As shown in Fig. 3.2, in the case of ($\theta = 0^\circ$) or ($m = 0$) the zigzag CNT is obtained.

An armchair CNT is constructed, in terms of chiral vector ($m = n$) or in terms of chiral angle ($\theta = 30^\circ$), as shown in Fig. 3.3.

Finally, a chiral CNT is formed if ($0^\circ < \theta < 30^\circ$) or ($m \neq n \neq 0$), as displayed in Fig. 3.4.

Thus, it results in three different configurations which include the chiral, zigzag and armchair CNT, as illustrated in Fig. 3.5.

As it is obvious, numerous types of CNTs, in the shape of zigzag, armchair and chiral, can be obtained with different chirality and diameters (see Fig. 3.6 3.7, and 3.8).

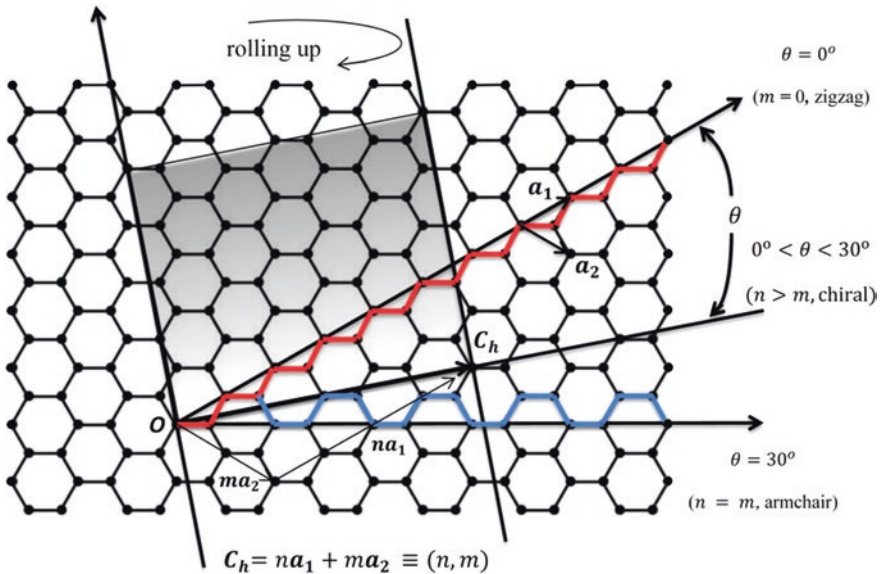


Fig. 3.1 Schematic of a graphene sheet and definition of geometrical parameters for describing a CNT

Based on the following equation, the diameter of the CNT can be calculated:

$$d_{\text{CNT}} = a_0 \sqrt{m^2 + mn + n^2} / \pi, \quad (3.2)$$

where $a_0 = \sqrt{3}b$ and $b = 0.142$ nm is the length of the C–C bond [46].

The circumference of the CNTs can be evaluated by the following equation [46]:

$$L = |C_h| = a \sqrt{n^2 + m^2 + nm} \quad (3.3)$$

In addition, the chiral angle is calculated by [46]:

$$\sin \theta = \frac{\sqrt{3}m}{2\sqrt{n^2 + m^2 + nm}} \quad (3.4)$$

$$\cos \theta = \frac{2n + m}{2\sqrt{n^2 + m^2 + nm}} \quad (3.5)$$

$$\tan \theta = \frac{\sqrt{3}m}{2n + m} \quad (3.6)$$

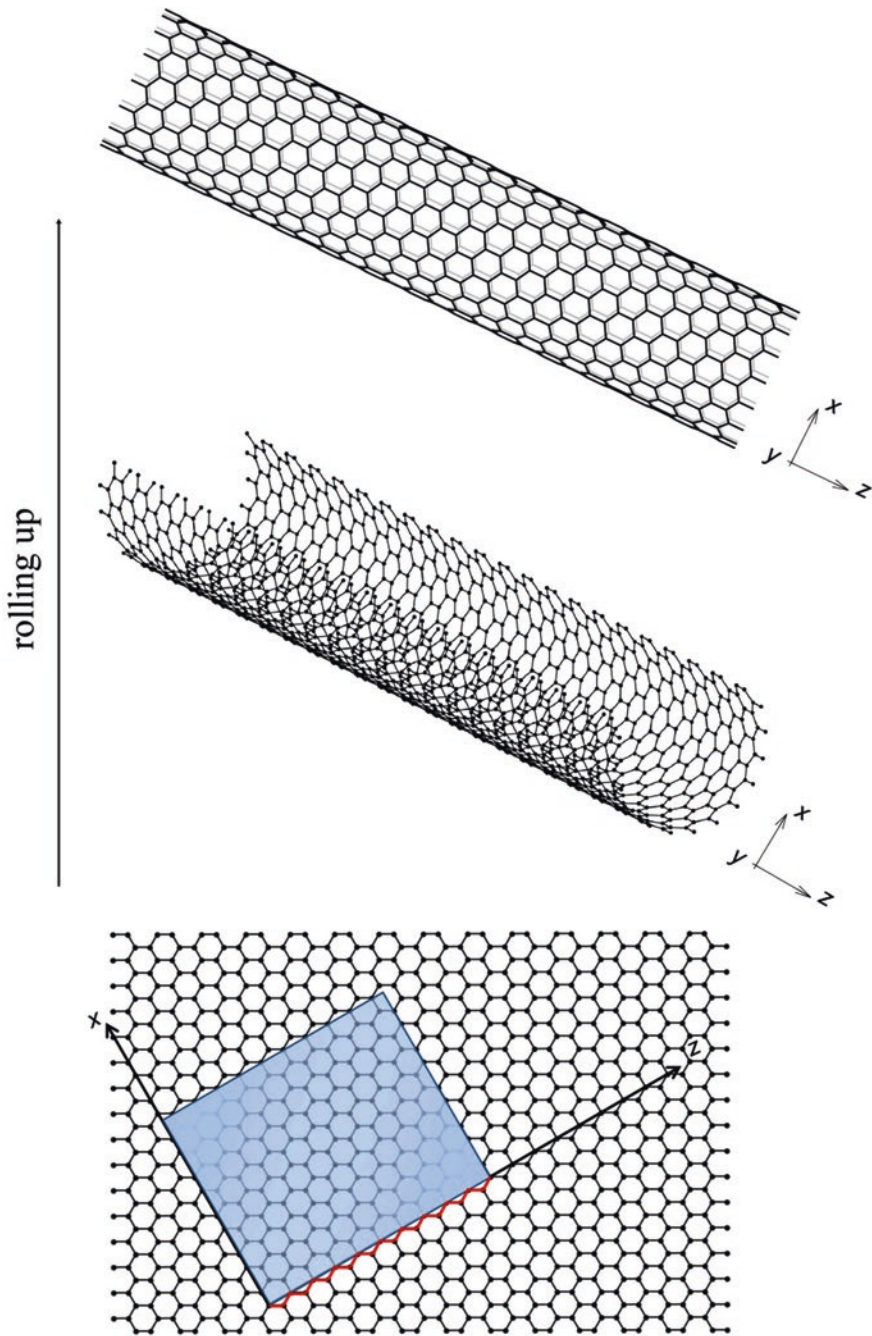


Fig. 3.2 Rolling up process of a graphene sheet into a zigzag tube

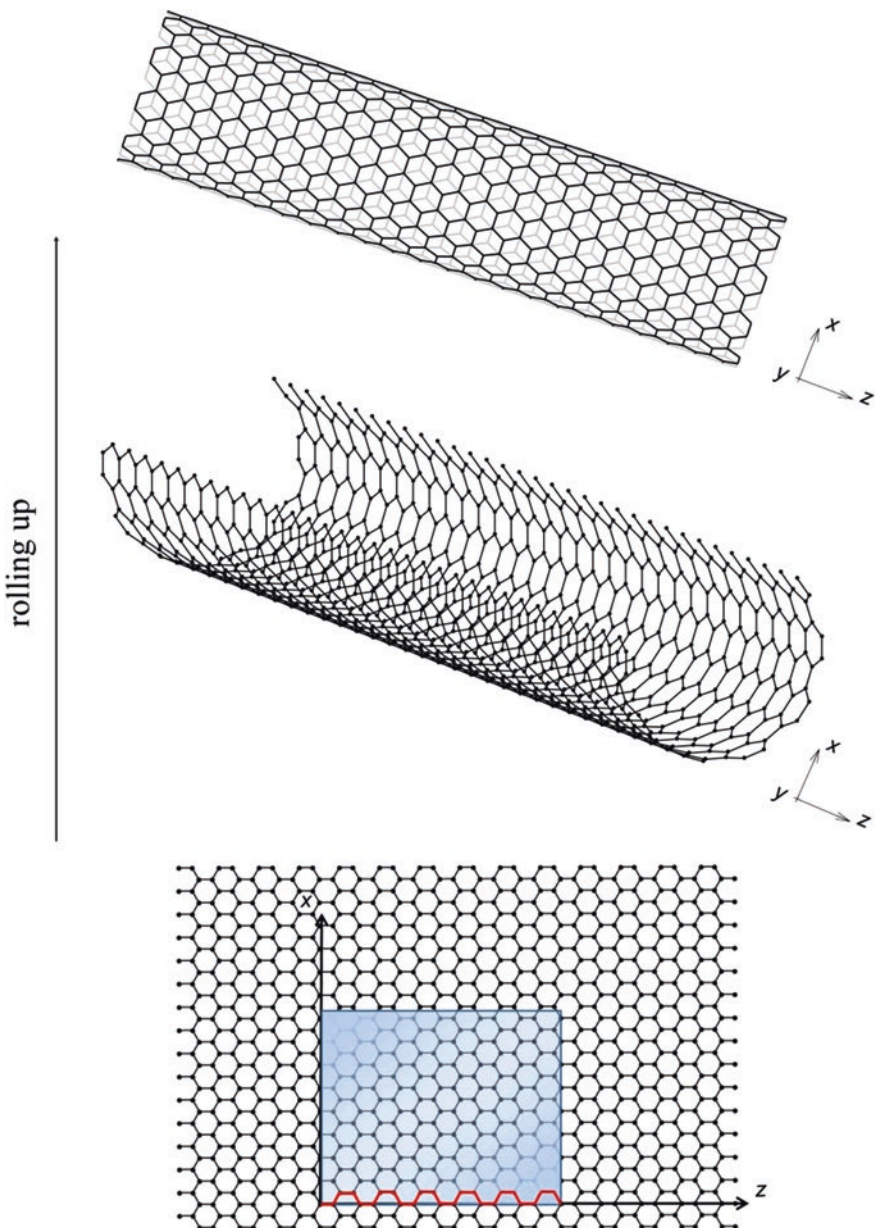


Fig. 3.3 Rolling up process of a graphene sheet into an armchair tube

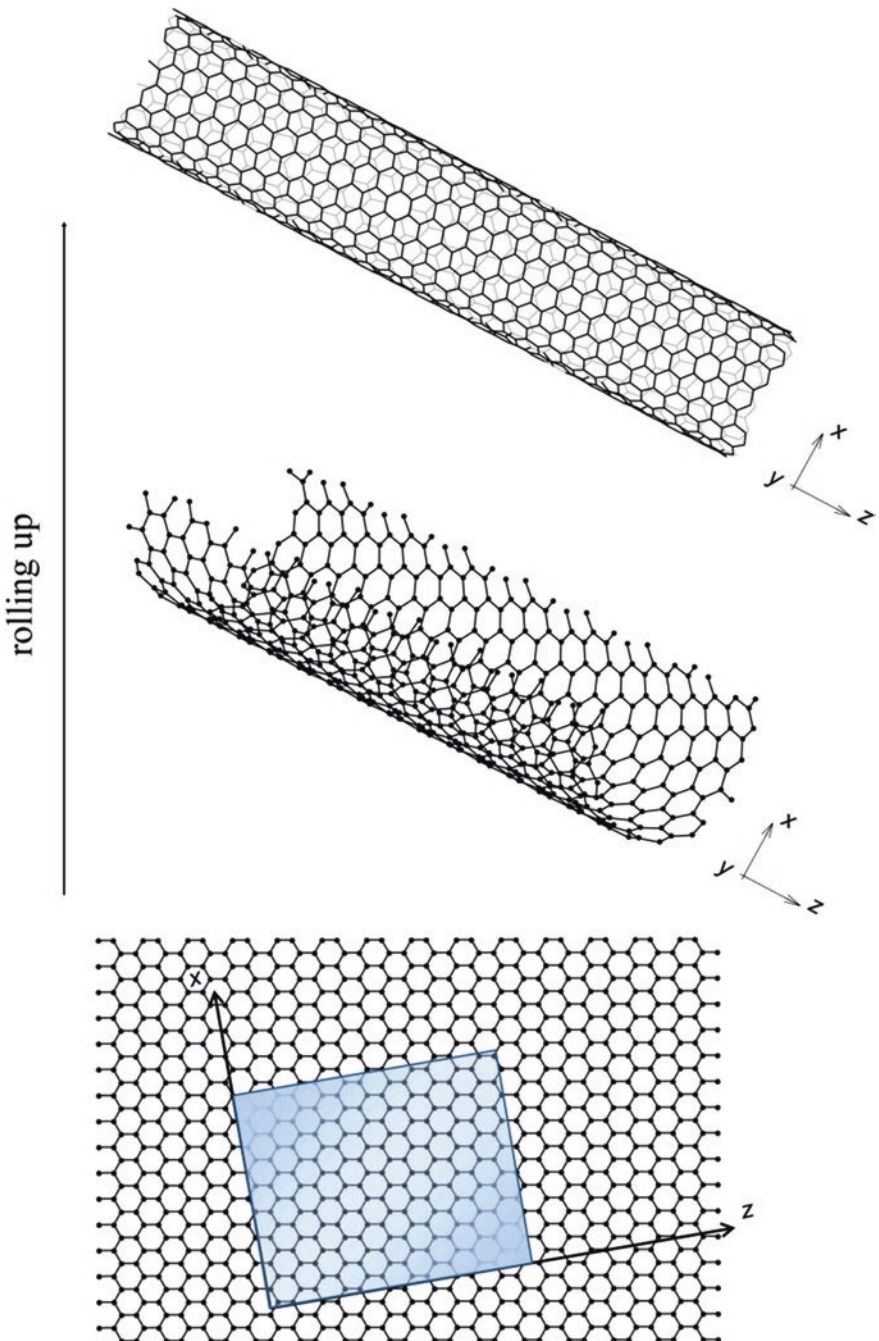


Fig. 3.4 Rolling up process of a graphene sheet into a chiral tube

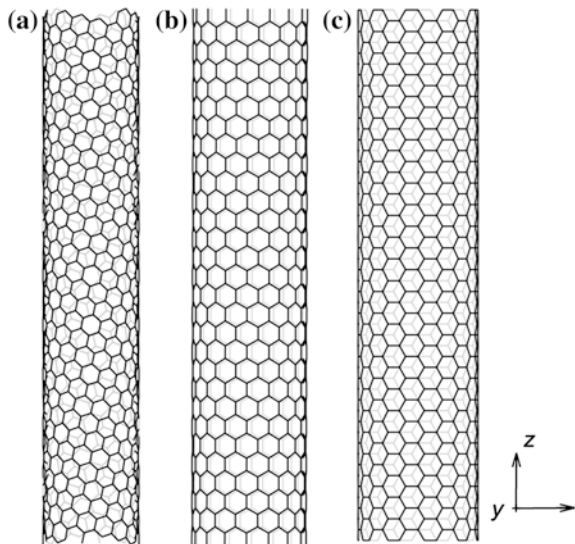


Fig. 3.5 Side view of the **a** (14,4)-chiral, **b** (16,0)-zigzag and **c** (10,10)-armchair CNTs

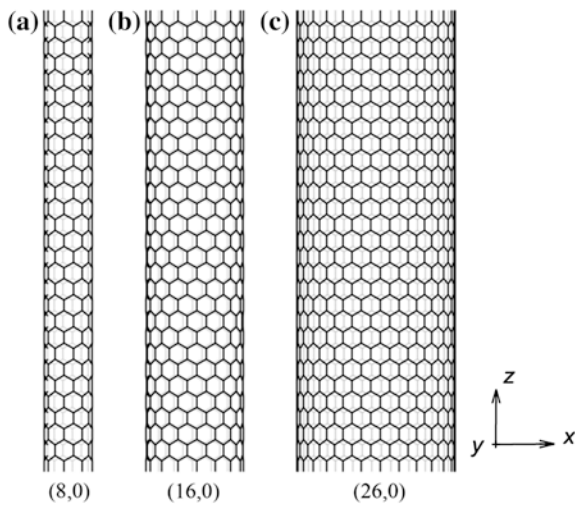


Fig. 3.6 Side view of **a** (8,0), **b** (16,0) and **c** (26,0) zigzag CNT

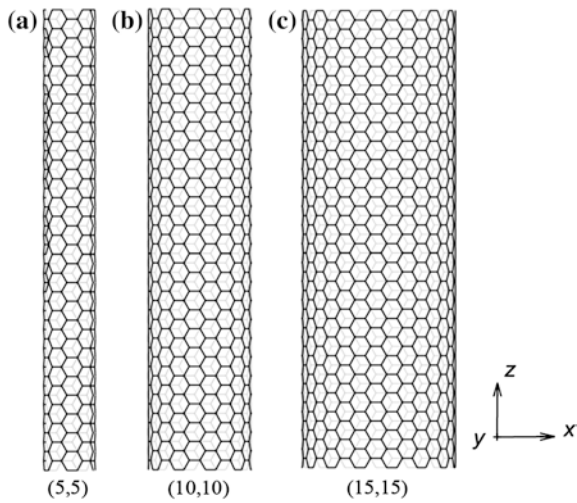


Fig. 3.7 Side view of **a** (5,5), **b** (10,10) and **c** (15,15) armchair CNT

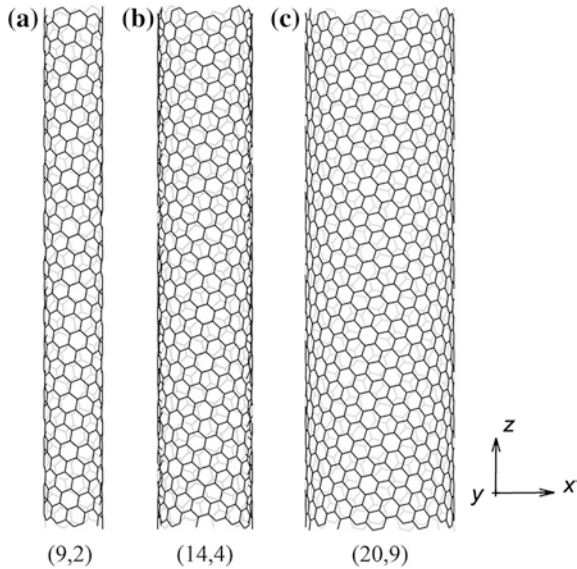


Fig. 3.8 Side view of **a**, **b** (14,4) and **c** (20,9) chiral CNT

Table 3.1 Some geometrical characteristics of different CNTs

CNT type	(n, m)	Tube length (nm)	Tube diameter (nm)	Chiral angle from zigzag direction θ (°)	Bond length
Zigzag	(8,0)	150	0.63	0	1.41
Zigzag	(16,0)	150	1.25	0	1.41
Zigzag	(26,0)	150	2.02	0	1.41
Armchair	(5,5)	150	0.68	30	1.41
Armchair	(10,10)	150	1.36	30	1.41
Armchair	(15,15)	150	2.03	30	1.41
Chiral	(9,2)	150	0.78	9.83	1.41
Chiral	(14,4)	150	1.27	12.22	1.41
Chiral	(20,9)	150	1.97	17.65	1.41

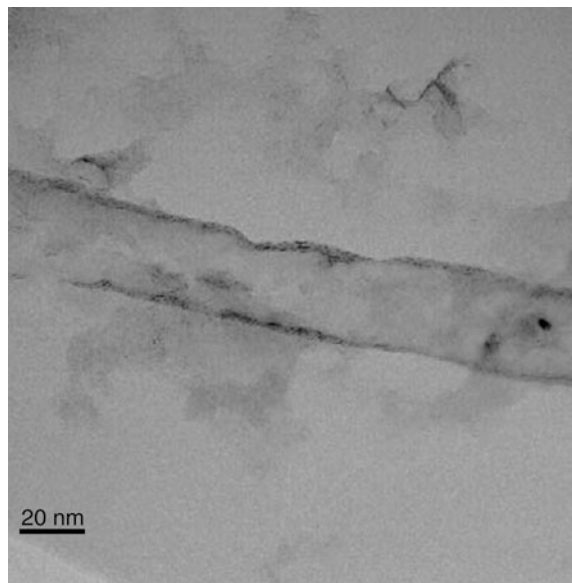
Fig. 3.9 Low magnification TEM micrograph from a straight nanotube [47]

Table 3.1 summarizes the characteristics of some zigzag, armchair and chiral CNTs.

Figure 3.9 illustrates a TEM image of a straight nanotube.

Chapter 4

Double and Multi-walled CNTs

Multi-walled carbon nanotubes (MWCNTs) consist of two or more SWCNTs with an interlayer of non-covalent van der Waals force acting between the carbon atoms of different walls. This force is also called the Lennard-Jones force [22]. Thus, for the simulation of a MWCNT, first the SWCNT configurations of the MWCNT are modeled. Then, the corresponding van der Waals force between them is defined by spring models. Since this weak non-covalent force has no material nature, a spring without mass is employed for the simulation of this force. Equation (4.1) represents the van der Waals force between two carbon atoms in the configuration of MWCNTs as a function of their distance and the change in distance after deformation:

$$F_{\text{vdw}} = 4\varepsilon/r[-12(\sigma/r)^{12} + 6(\sigma/r)^6] + k\Delta r \quad (4.1)$$

where $\sigma = 0.3851 \text{ nm}$ and $\varepsilon = 0.4396 \text{ kJ mol}^{-1} = 0.072997284 \times 10^{-20} \text{ J}$ are the Lennard-Jones parameters, r is the distance and Δr is the change in the distance between two carbon atoms which is as a result of an external force, applied on the structure and the consequent CNT deformation and change in the location of the atoms. The spring stiffness $k = 0.24245 \text{ N/m}$ is evaluated by choosing two points from the Lennard-Jones force diagram in the domain $0.33 < r < 0.38 \text{ nm}$ [22]. The diagram of the Lennard-Jones force interaction between two carbon atoms is illustrated in Fig. 4.1.

Figure 4.2 shows the geometry of zigzag and armchair MWCNTs.

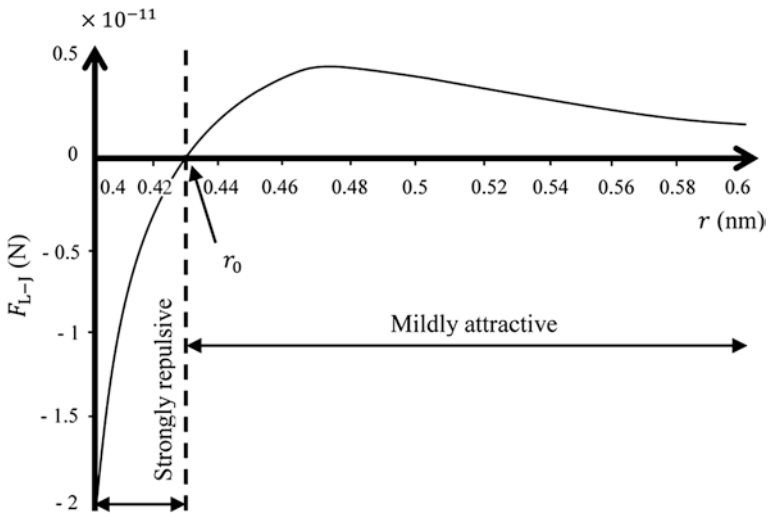


Fig. 4.1 Lennard–Jones force diagram, adopted from [48]

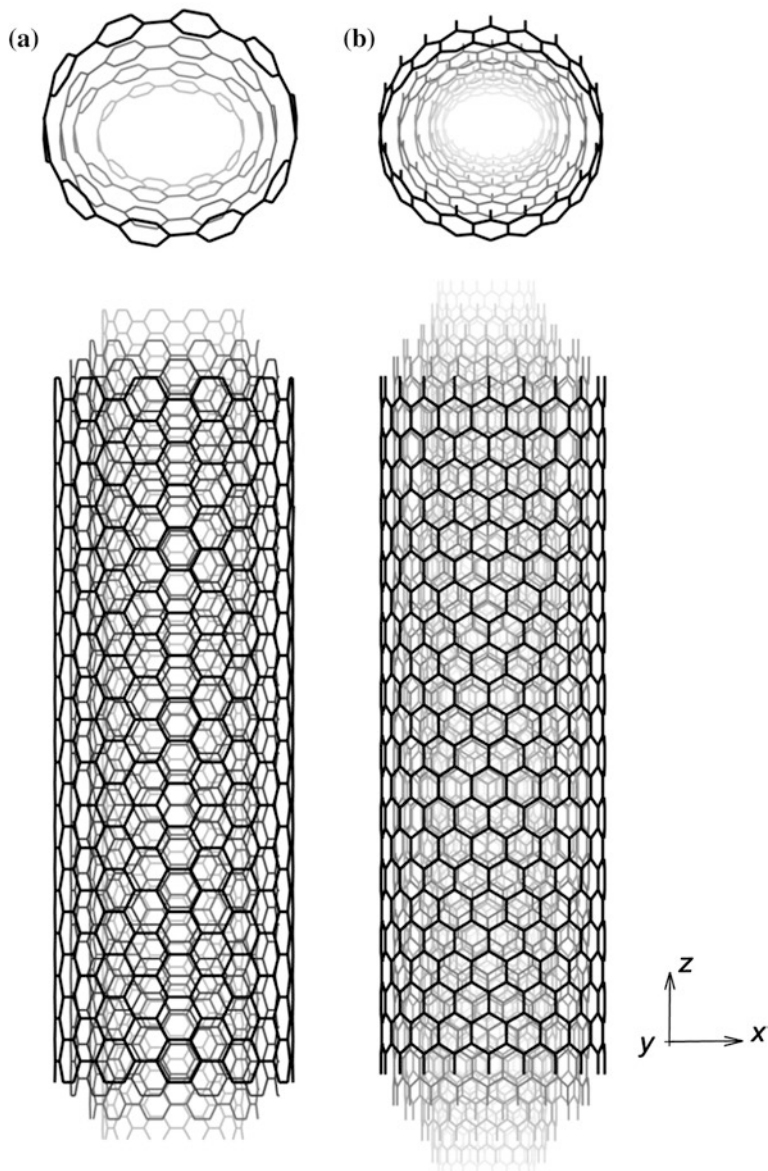


Fig. 4.2 Front view and a single ring of **a** (10, 10)-armchair 4-walled and **b** (20, 0)-zigzag 6-walled CNT

Chapter 5

Defective CNT Structures

Basically, the defects in the configuration of CNTs are categorized as macroscopic and atomic modifications. The following section will explain the differences between these two types of defects in detail. Figure 5.1 illustrates a few instances of these modifications.

5.1 Macroscopic Modifications

A homogeneous CNT can be viewed as a rolled graphene sheet with specified width, while a hetero-junction CNT, treated as a wrapped graphene sheet with specific geometry, is created by connecting two CNTs through the introduction of Stone-Wales defects (pentagon and heptagon pair defects) into the connecting region, as shown in Fig. 5.2.

5.1.1 Straight Hetero-Junctions

It is possible to connect two CNTs with different chiralities by just introducing a pair of pentagon and heptagon defects in the otherwise perfect hexagonal graphite lattice [49]. Hetero-junction CNTs are classified based on the configurations of their two constituent homogeneous CNTs. For instance, a hetero-junction CNT created by connecting a (7,7)-armchair CNT and a (9,9)-armchair CNT is referred to as a (7,7)-(9,9) hetero-junction CNT [50]. Basically, the connecting region of hetero-junctions is classified into three different categories, i.e. large angle, small angle and straight connections. Depending on the type of the fundamental CNTs of these specific configurations, the hetero-junctions are categorized as straight structures and bending models, i.e. if the constituent CNTs of a hetero-junction are

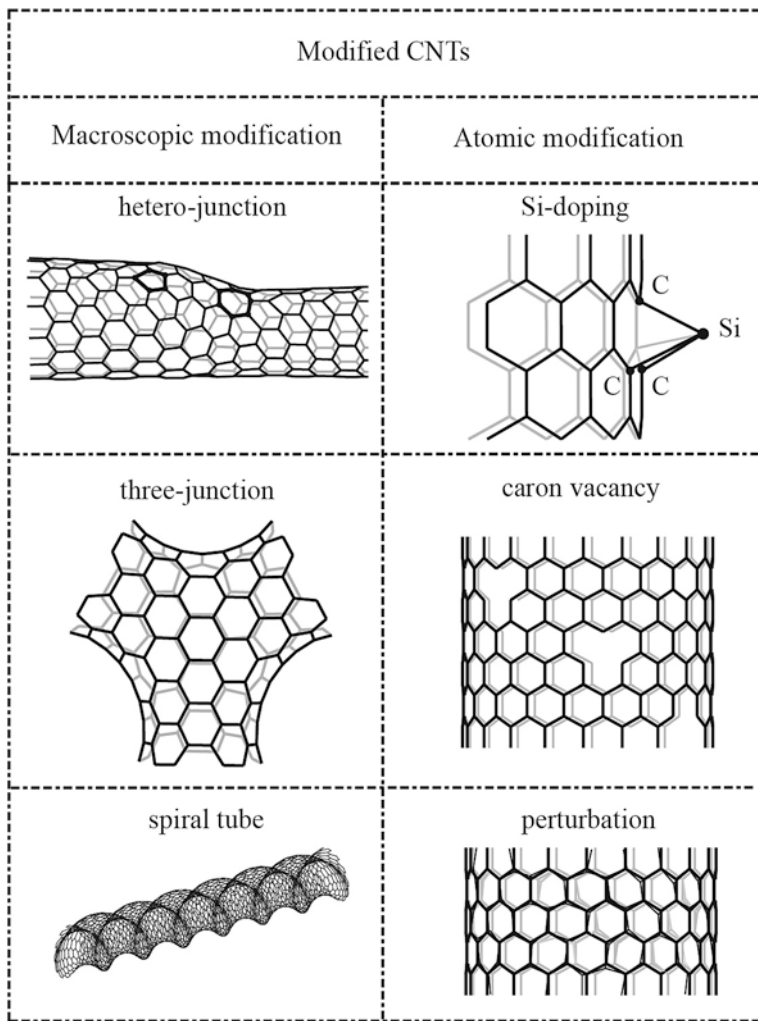


Fig. 5.1 Some examples of macroscopic and atomic modifications

in the same type (either armchair, zigzag and chiral), the configuration of the hetero-junction is sorted as a straight model and the homogeneous CNTs will be connected with parallel longitudinal axis. On the other hand, if the fundamental CNTs of a hetero-junction are not in the same type, the structure of the hetero-junction will be created with a bending angle. This type of structure is called a kink hetero-junction. Figure 5.3 illustrates some models of straight hetero-junctions with different types of the fundamental homogenous CNTs.

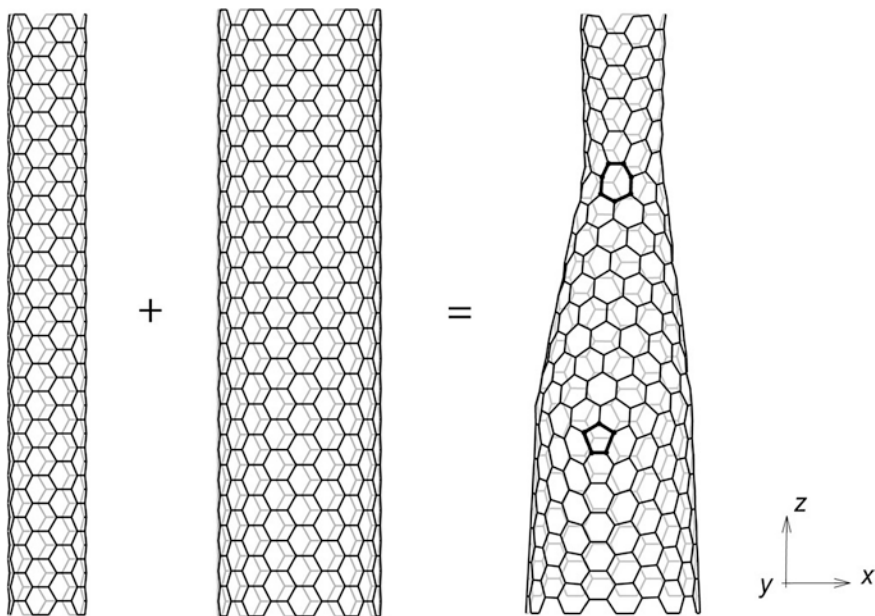


Fig. 5.2 Front view of (5,5)-(10,10) hetero-junction carbon nanotube with pentagon-heptagon (5-7) pair defects

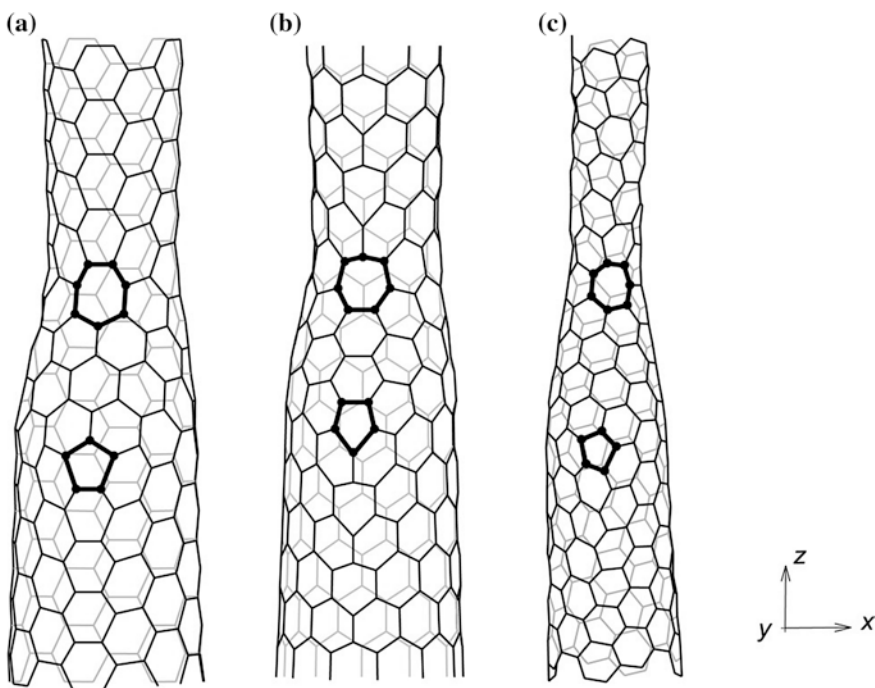


Fig. 5.3 Pentagon-heptagon pair defects of **a** (5,5)-(7,7), **b** (9,0)-(11,0) and **c** (5,2)-(8,4) hetero-junction CNTs

5.1.2 Kink Hetero-Junctions

As it is noticeable, the pentagon-heptagon pair defects of straight hetero-junctions both appear in one side of the configuration. In contrast, the pentagon-heptagon pair defects of kink hetero-junctions with bending angles are placed separated in the front and back side of these specific structures. Figure 5.4 shows a kink hetero-junction which is constructed by the junction of an armchair and zigzag homogenous CNT.

The geometry of a hetero-junction CNT is more sophisticated as compared with that of a CNT owing to the irregular configuration of the connecting region. In the case of the straight hetero-junctions, the axis of the wider CNT is defined as the reference axis of the junction because of the fact that the two fundamental CNTs of a hetero-junction are able to align on a planar surface. In the case of kink

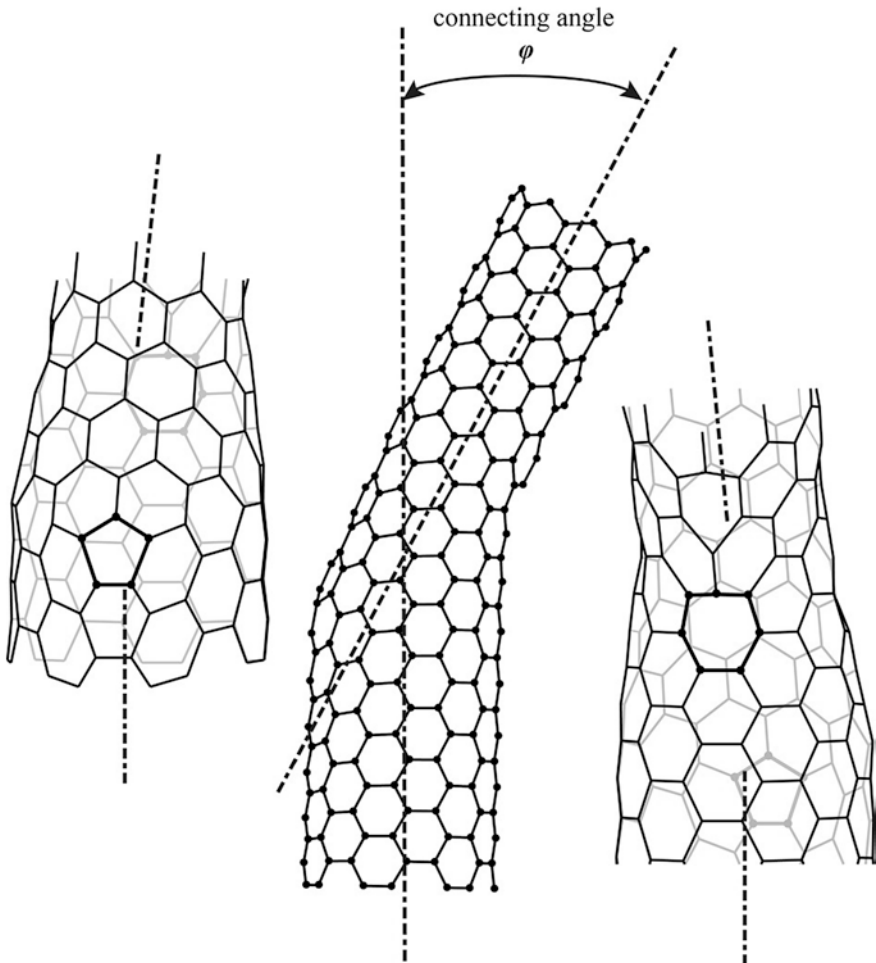


Fig. 5.4 Pentagon-heptagon pair defects of (7,7)-(9,0) kink hetero-junction CNT

hetero-junctions with bending formation, the angle between two homogeneous CNTs joined by a kink junction is variable from 12° to 45° which can be changed based on the chirality of the constituent CNTs. The angle can be made smaller by placing the pentagon and heptagon closer to each other [51]. This angle is caused by the change of the structural arrangement of two different CNTs with different chirality, as displaced in Fig. 5.5.

The overall length of a straight hetero-junction is defined as (see Fig. 5.6):

$$l = l_{\text{thin}} + l_{\text{connecting}} + l_{\text{wide}} \quad (5.1)$$

where l_{thin} , $l_{\text{connecting}}$, and l_{wide} are the length of the thinner tube, the connecting region and the wider tube, respectively. By the geometries of the connected CNTs,

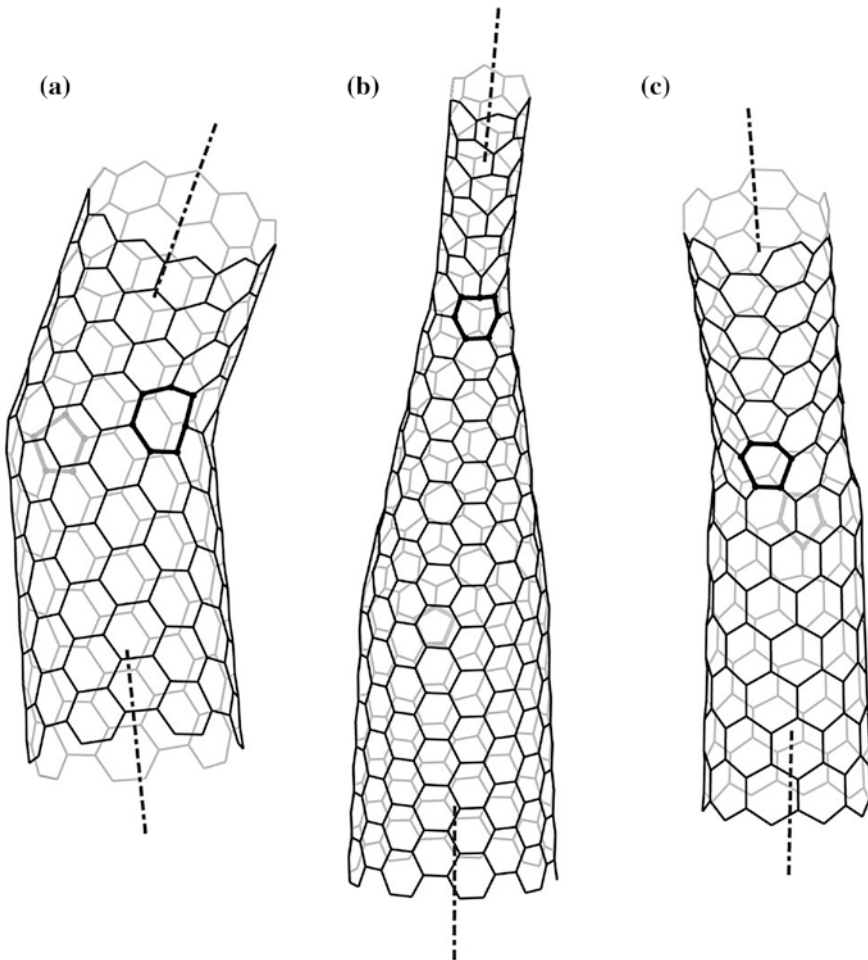


Fig. 5.5 Pentagon-heptagon pair defects of **a** (11-0)-(7,7), **b** (9,9)-(6,0) and **c** (5,5)-(10,0) hetero-junction CNTs

the length of the connecting region can be approximately obtained based on the simplified geometry of a right-angled triangle as [50]:

$$l_{\text{connecting}} = \frac{\sqrt{3}}{2} \pi (d_{\text{wide}} - d_{\text{thin}}) \quad (5.2)$$

where d_{wide} and d_{thin} are the diameters of the wider and thinner tubes, respectively (see Fig. 5.6).

As the junction may consist of two homogeneous CNTs with different diameters, we define the diameter of junction as the average diameter of both CNTs, i.e.

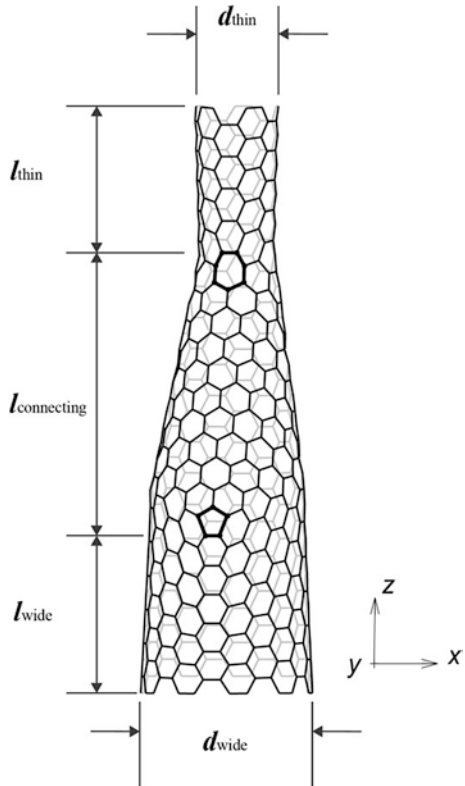
$$\bar{d} = \frac{1}{2} (d_{\text{wide}} + d_{\text{thin}}) \quad (5.3)$$

The aspect ratio of the junction is defined as [50]:

$$\eta = \frac{l}{\bar{d}} \quad (5.4)$$

Another method to distinguish hetero-junctions can be according to the difference in carbon atoms per cross section. This difference is calculated by subtracting the number of carbon atoms of the thinner tube's cross section from those of the wider

Fig. 5.6 Specification of (5,5)-(10,10) hetero-junction CNT



tube's cross section [52]. As illustrated in Fig. 5.7, the difference between the number of carbon atoms of the thinner and the wider tube's cross sections could be calculated.

Table 5.1 represents the characteristics of some hetero-junction CNTs.

Some types of CNTs are called metallic and some of these carbon nanostructures are semiconductors. As illustrated in Fig. 5.8, the metallic and semiconductor tubes are denoted by circled dots and simple dots, respectively.

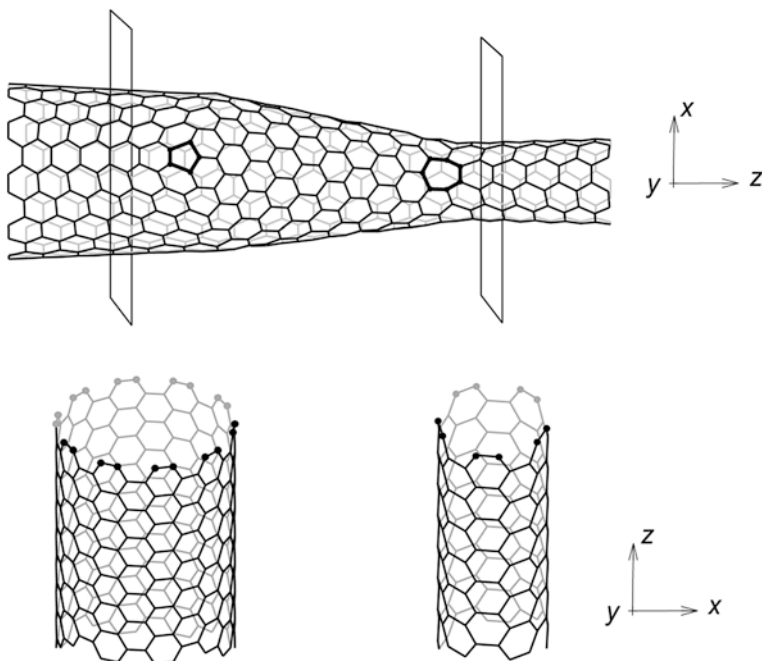


Fig. 5.7 The difference between the number of carbon atoms of the thinner and the wider tube's cross sections

Table 5.1 Some features of hetero-junction CNTs

Chirality (n,m) (n',m')	Difference in C-atoms per cross section	Diameter of the junction \bar{d} (nm)
(3,3)-(5,5)	4	0.539
(5,5)-(7,7)	4	0.808
(7,7)-(9,9)	4	1.707
(5,5)-(10,10)	10	1.010
(9,9)-(11,11)	4	1.346
(9,0)-(12,0)	3	0.816
(11,0)-(12,0)	1	0.894
(12,0)-(16,0)	4	1.088
(14,14)-(16,16)	4	2.020

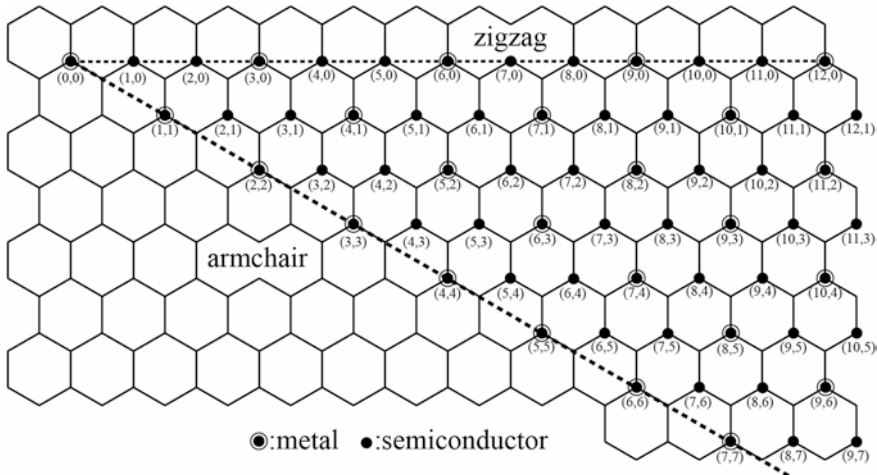


Fig. 5.8 Possible vectors for chiral tubes, adopted from [53]

The condition for a tube to be metallic is:

$$2n_1 + n_2 = 3q \quad (5.5)$$

where n_1 and n_2 are the unit vectors of the graphene sheet, and q is an integer. In particular, all armchair CNTs are metallic, and zigzag tubes are metallic when n_1 is a multiple of three.

Figures 5.9, 5.10, 5.11, 5.12, and 5.13 illustrate the configuration of some hetero-junction CNTs with pentagon and heptagon pair defects. By introducing these pair defects at two diametrically-opposed sides of the structure, the axis of the two connected nanotubes make an angle around 35° . Bending angles of that order of magnitude have been observed experimentally by TEM [54]. It is possible to have a smaller angle by locating the pentagon and heptagon closer to each other [51]. In addition, it is practical to connect two different nanotubes without bending the structure by aligning the pentagon and heptagon along the same side [55].

Table 5.2 describes the classification of these hetero-junction CNTs.

Large-angle connections

(5,5)-(9,0)

The (5,5)-(9,0) knee, as shown in Fig. 5.9, connects a nanotube with the perpendicular orientation (bottom) to one with the parallel orientation (top). The diameters of the two junctions is close to 0.35 nm and the bending angle is 36° . This hetero-junction is categorized as a metal-metal nanostructure.

(6,6)-(10,0)

As illustrated in Fig. 5.10, the (6,6)-(10,0) knee is a semiconductor-metal hetero-junction. The bending angle of this nanoparticle is 35° .

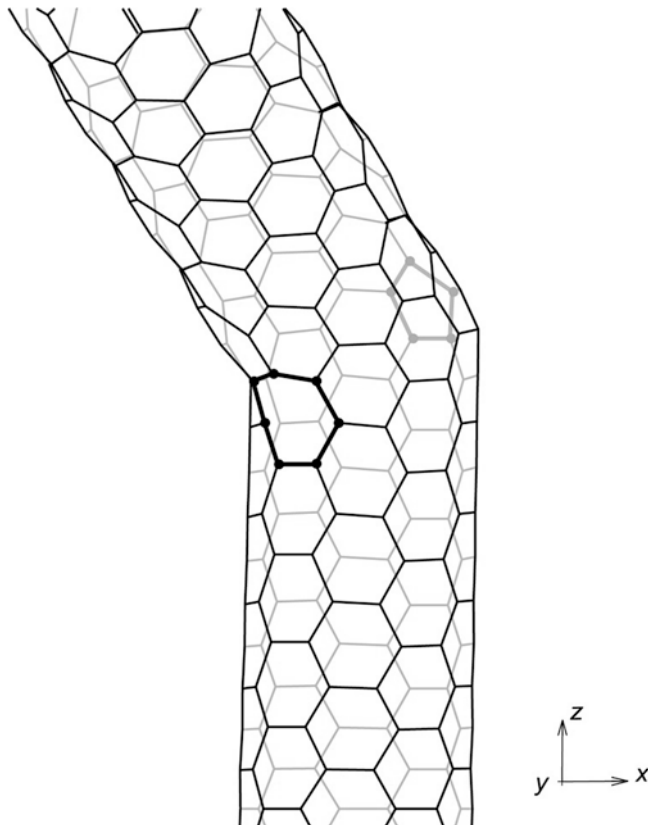


Fig. 5.9 Pentagon and heptagon pair defects of a (5,5)-(9,0) hetero-junction CNT

Small-angle connections

(8,0)-(7,1)

The lower half of this hetero-junction is a semiconductor and the upper part is a metallic chiral nanotube. The bending angle of this hybrid is 12° [56]. Figure 5.11 illustrates the model of (8,0)-(7,1) hetero-junction CNT.

Straight connection

(9,0)-(12,0)

As shown in Fig. 5.12, this specific type of hybrid is constructed with a pair of pentagon and heptagon defects. This system, which connects two quasi-metallic zigzag tubules, has been considered for tunneling conductance calculations [57].

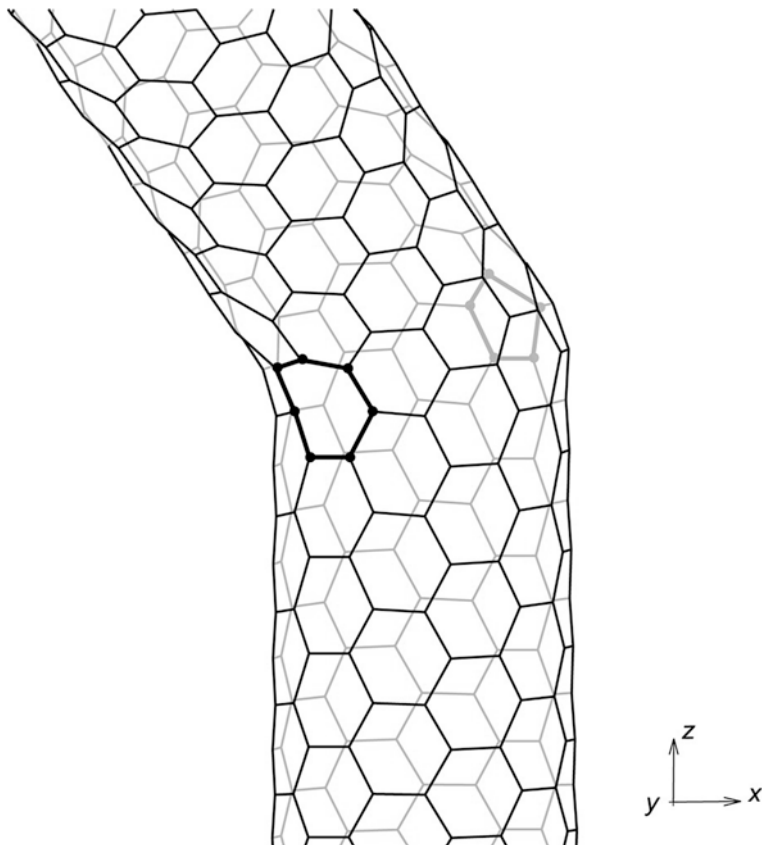


Fig. 5.10 Pentagon and heptagon pair defects of a (6,6)-(10,0) hetero-junction CNT

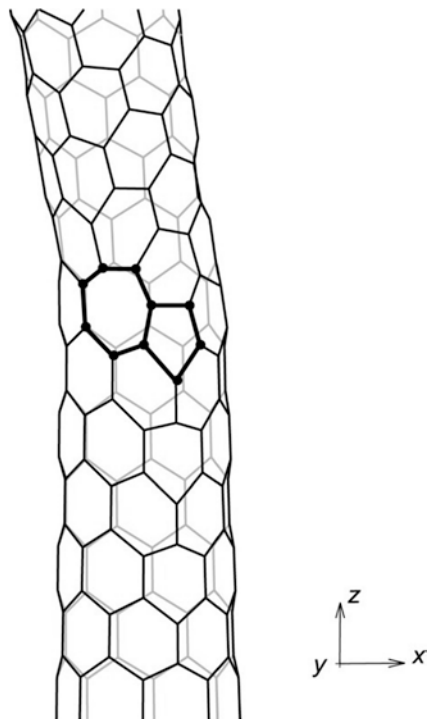
(11,0)-(12,0)

This hetero-junction is a semiconductor-metal hybrid. Two junctions with parallel (or zigzag) orientation are connected with a pair of edge-sharing pentagon and heptagon oriented parallel to the tubule axis. Figure 5.13 illustrates this type of hybrid.

5.1.3 Three-Nanotube Junctions

The construction procedure becomes much harder when we join three CNTs together to form a three-tube configuration [41]. As illustrated in Fig. 5.14, the structure is now composed of three branches, and the transition between three tubes demands a particular geometry which cannot be arbitrary.

Fig. 5.11 Pentagon and heptagon pair defects of a (8,0)-(7,1) hetero-junction CNT

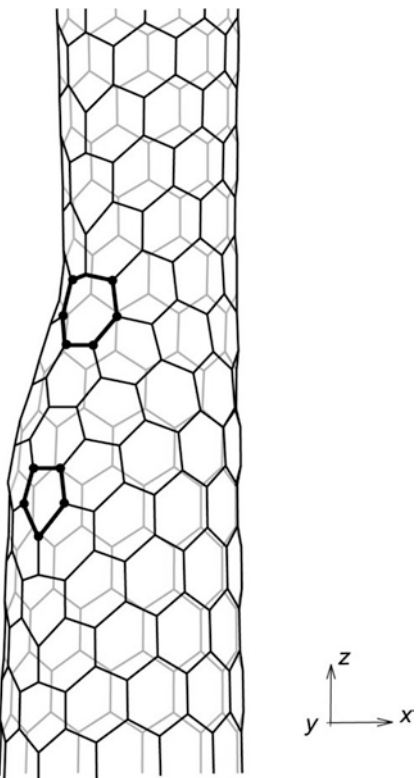


Three joined tubes require at least six heptagons, which have to be placed adequately for each specific junction. Nevertheless, it is not possible in every situation to guess the placement of the heptagons, and this task becomes a mathematical puzzle which is quite hard to solve. Figure 5.15 shows the heptagon defects of a three-CNT junction. One of the main potential applications of these nanoparticles can be in the micro- and nanofluidic systems. For example, they can be applied as blood vessels or as flow sensors in the nano-measurement approaches. Also, they may have some other applications in the nanoelectronics and nanomechanics similar to those for the CNTs. Junctioned CNTs can be the building blocks of the nanoelectronic devices made entirely of carbon [45]. Moreover, they can be used in nano-heat transfer.

5.1.4 Curvature

Curvature is also an important structural defect in structure of CNTs which affect the mechanical properties of these nanostructures. According to experimental and modeling results, one of the key aspects of CNTs which should be properly

Fig. 5.12 Pentagon and heptagon pair defects of a (9,0)-(12,0) hetero-junction CNT



addressed is initial curvature [49]. Figure 5.16 illustrates the models of CNTs which were simulated from straight structure to curved CNT with 45° bending angle.

Figure 5.17 illustrates the TEM image of a bending carbon nanotube.

5.1.5 Twisting

CNTs might be deformed by a twisting angle in reality. This particular modification affects the mechanical properties of CNTs [59]. Figure 5.18 illustrates the configuration of CNTs which were simulated from straight model to twisted CNT with a 10° twisting angle.

Fig. 5.13 Pentagon and heptagon pair defects of a (11,0)-(12,0) hetero-junction CNT

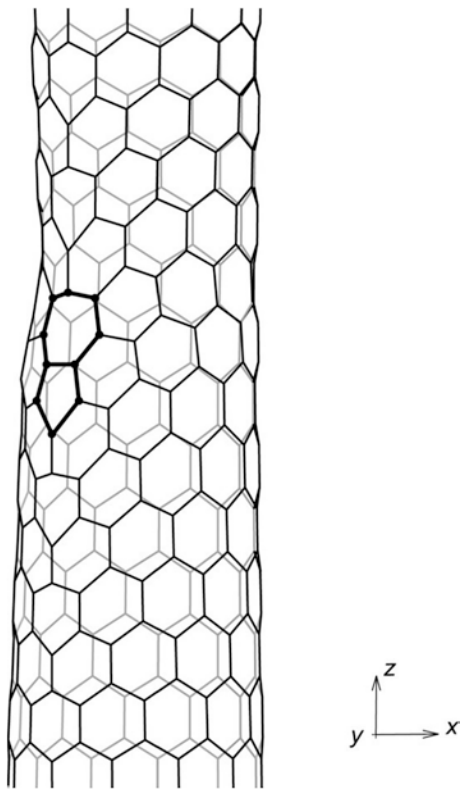


Table 5.2 Classification of hetero-junction CNTs

Type of connection	Chirality	Connecting angle (°)
Large-angle connections	(5,5)-(9,0) (6,6)-(10,0)	36 35
Small-angle connections	(8,0)-(7,1)	12
Straight connection	(9,0)-(12,0) (11,0)-(12,0)	0 0

5.1.6 Spiral Deformation

Another type of defect is spiral deformation which happens when a CNT is twisted like a spring along its longitudinal axis [60], as shown in Fig. 5.19.

Based on this spiral angle, numerous CNTs can be formed with different configuration, as illustrated in Fig. 5.20.

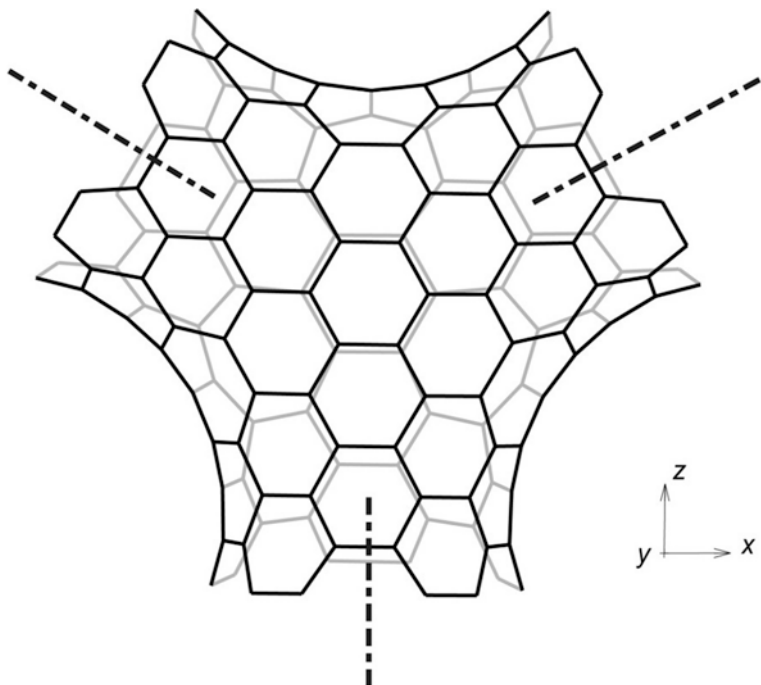


Fig. 5.14 Side view of a three-CNT junction

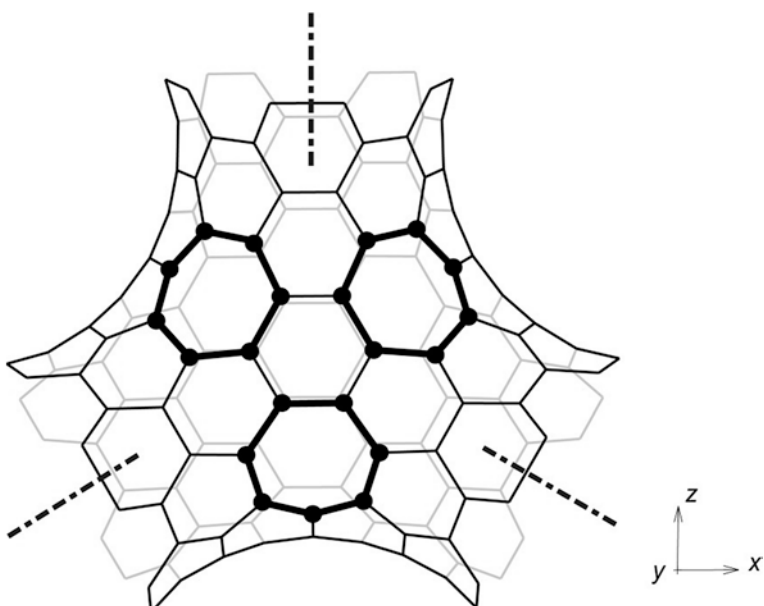


Fig. 5.15 The placement of the heptagon defects of a three-CNT junction

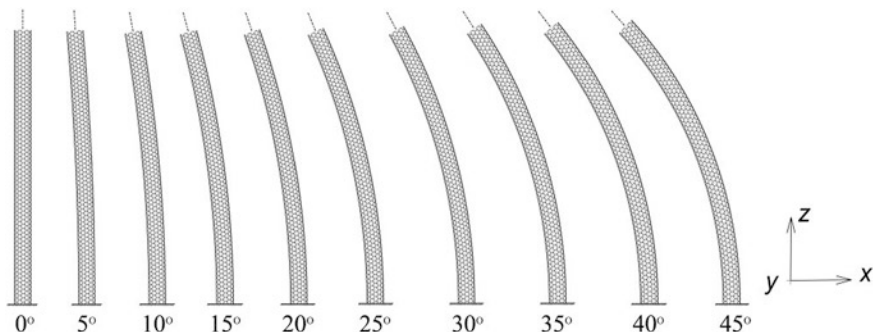


Fig. 5.16 (8,8)-armchair CNTs with fixed-free boundary condition and different curvature from 0° to 45° bending angle

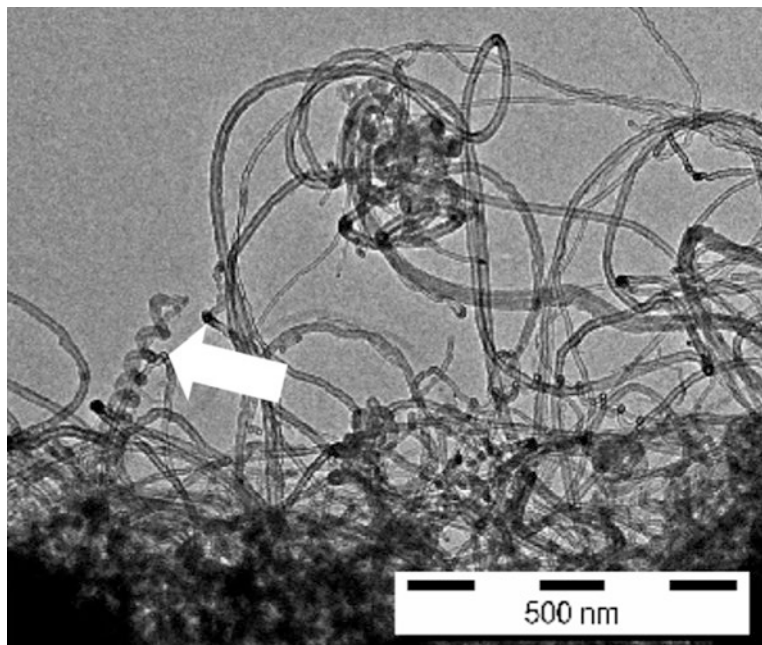


Fig. 5.17 TEM image of coiled and bent CNTs [58]

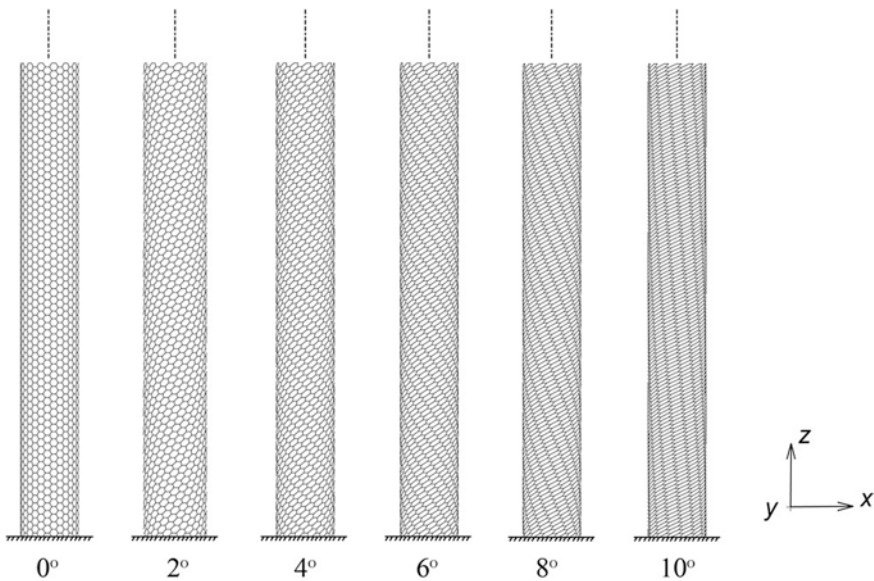


Fig. 5.18 (16,16)-armchair CNTs with fixed-free boundary condition and different twisting angle from 0° to 10° along their longitudinal axis

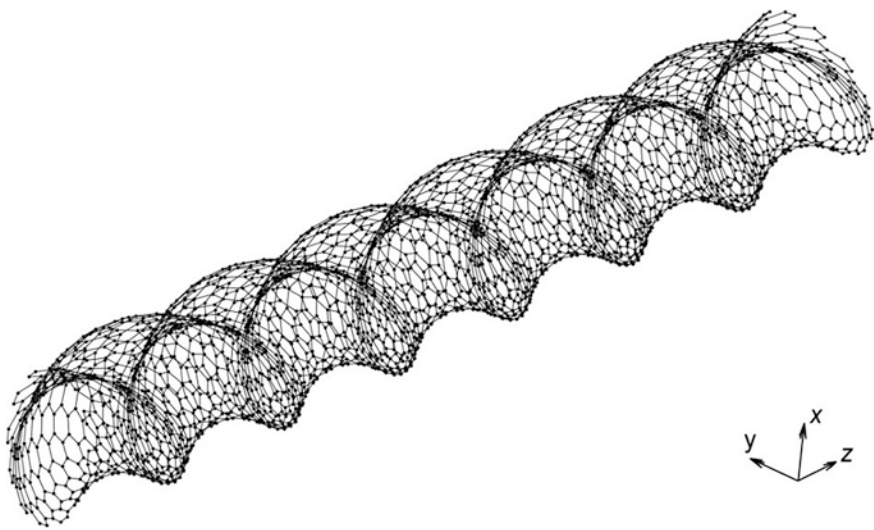


Fig. 5.19 General view of a spiral armchair CNT

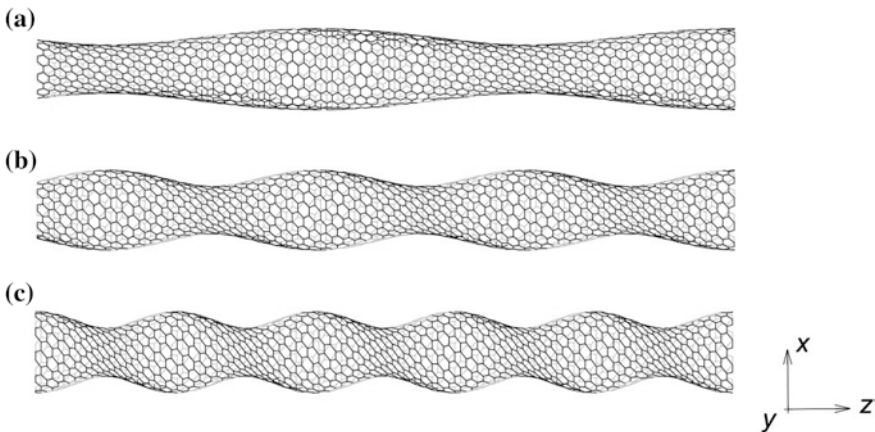


Fig. 5.20 (10,10) spiral armchair CNT with **a** 2°, **b** 4° and **c** 6° twisting angle

5.2 Atomic Modifications

Apart from the macroscopic defects in the configuration of CNTs, there are other kinds of defects, e.g. Si-doping, carbon vacancy and perturbation, which might impure the structure of perfect CNTs.

5.2.1 Doping

This random imperfection corresponds to the case where a finite number of carbon atoms were replaced by silicon, nitrogen, boron, etc. [61–63], as illustrated in Fig. 5.21 for the silicon atom.

5.2.2 Carbon Vacancies

In this case, a finite number of carbon atoms were removed from the structure of CNTs, as shown in Fig. 5.22.

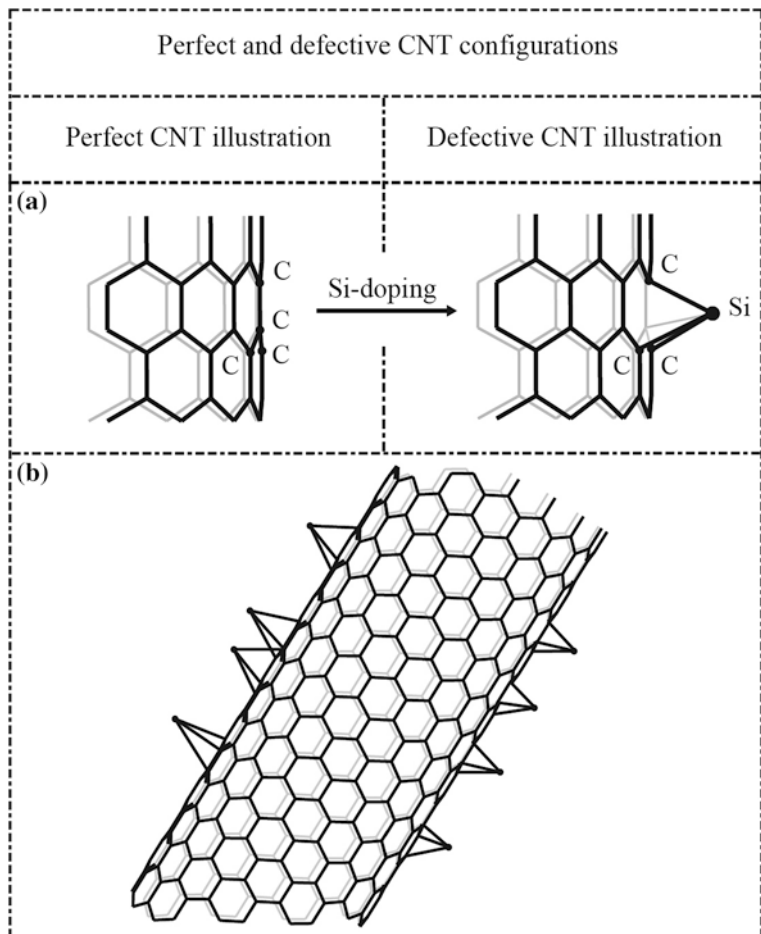


Fig. 5.21 **a** Si-doping of a perfect zigzag CNT and **b** global view of a Si-doped zigzag single-walled carbon nanotube

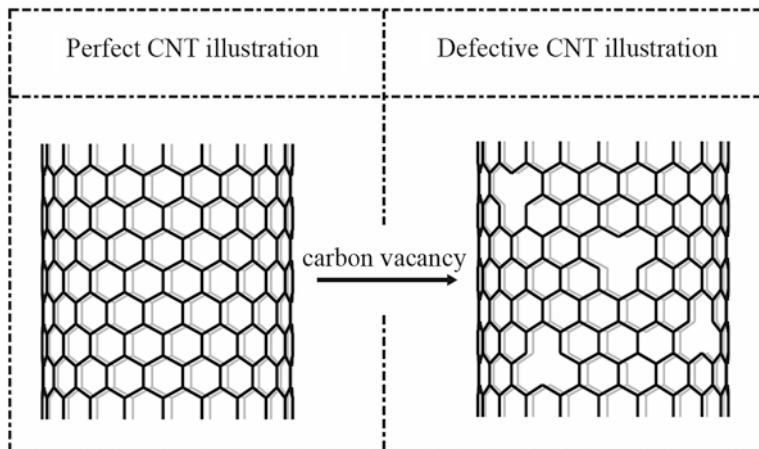


Fig. 5.22 Carbon vacancy of a perfect zigzag CNT

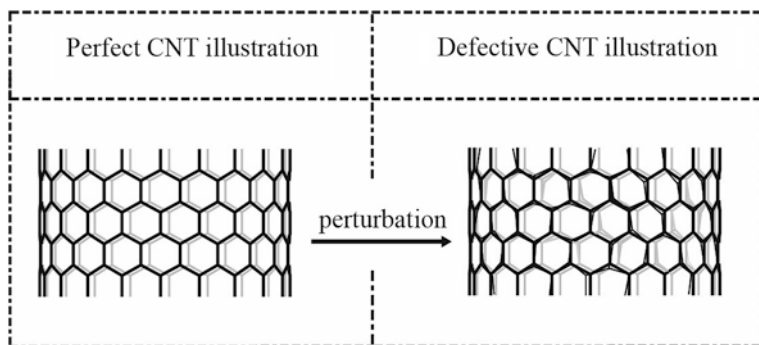


Fig. 5.23 Perturbation of a perfect zigzag CNT

5.2.3 Perturbation

In this situation, all carbon atoms of the structure were misplaced for a random length, as displayed in Fig. 5.23.

Chapter 6

Degenerated Tubes

Beside carbon nanotubes, there are some other configurations of nanostructures, such as nanocones, capped CNTs, fullerene molecules, etc.

6.1 Carbon Nanocone Structures

These specific types of nanostructures were reported to possess a wide distribution of apex angles, which support a disclination model for cone-helix structures [64]. The cone-helix configuration is successful in predicting the expected apex angles of graphite cones synthesized under various laboratory conditions and formed naturally from fluids during metamorphism shape. It was reported in [65] that there are five possible apex angles that are geometrically permitted by inserting pentagons from one ring to five rings into the hexagonal framework. Due to possessing a sharp tip which can be used to achieve particular mechanical characteristics, nanocones are interesting materials for technological applications. These nanoparticles occur on the surface of natural graphite. Nanocones are distinguished based on their disclination angle d_θ which is defined as the angle of the sector removed from a flat sheet to form a cone. For carbon nanocones, we analyzed three disclination, $d_\theta = 120^\circ$, 180° , and 240° , as illustrated in Fig. 6.1.

The generated single-walled carbon nanocone (SWCNC) structures are shown in Fig. 6.2. The apex angles of nanocones that are made in this manner can also be given by $2 \arcsin(1 - [d_\theta]/360)$, where d_θ is the disclination angle in degrees. Taking d_θ from 120, 180 and 240, the apex angles of cones are 83.6° , 60° , and 38.9° [66].

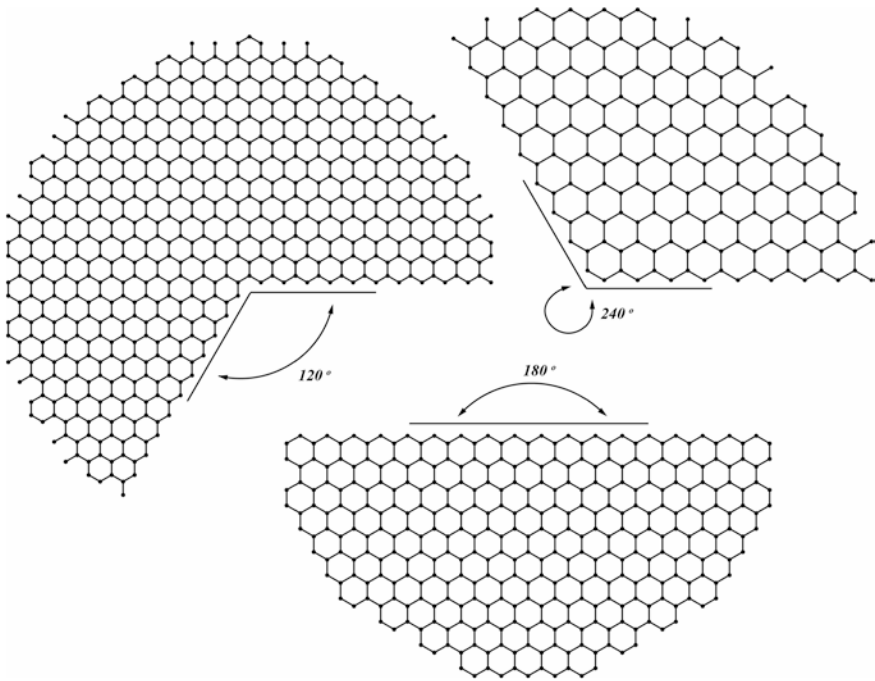


Fig. 6.1 Cone sheets with disclination angles of 120° , 180° , and 240°

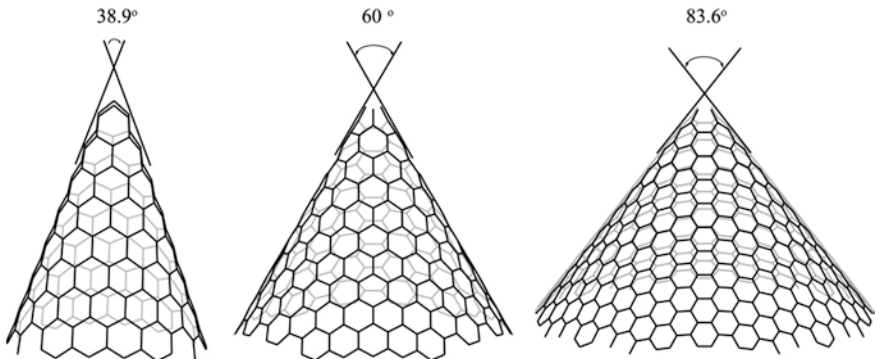


Fig. 6.2 Cones with apex angles of 38.9° , 60° , and 83.6°

6.2 Buckminsterfullerene

Buckminsterfullerene (or Bucky-balls) is some kind of spherical-shaped fullerene molecule which has cage-like fused-ring configurations [67]. Figure 6.3 illustrates a model of buckminsterfullerene.

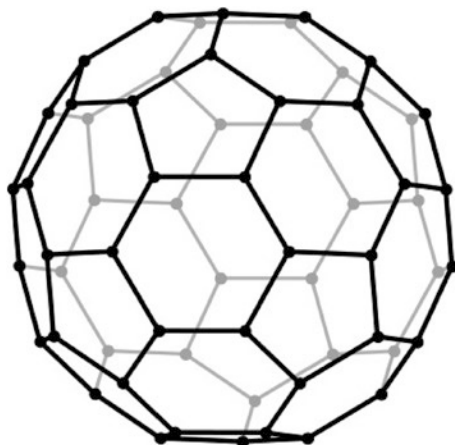


Fig. 6.3 A frame-like structure of buckminsterfullerene

6.3 Capped CNTs

By rolling up a graphene sheet as a cylinder and capping each side of the cylinder with half of the fullerene molecule, a capped CNT is modeled. Figure 6.4 shows single-walled armchair and zigzag capped CNTs.

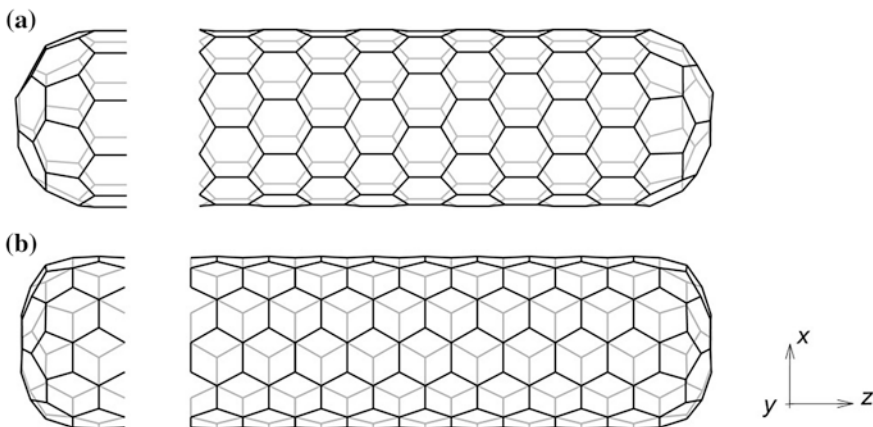


Fig. 6.4 Side view of **a** armchair and **b** zigzag capped CNT

Chapter 7

Finite Element Modeling

7.1 Material and Geometric Properties

In a CNT, carbon atoms are bonded together by covalent bonds which have their specific lengths and angles in a three-dimensional space. It was assumed that CNTs, when subjected to loading, behave like space-frame structures. Thus, the bonds between carbon atoms are considered as connecting load-carrying generalized beam members, while the carbon atoms act as joints of the members [20]. This idea is illustrated in Fig. 7.1.

7.2 Geometry Generation

For macroscopic space frame configurations in the scope of classical structural mechanics, the material properties (e.g. Young's and shear moduli) and element sectional parameters (e.g. second moment of area) can be easily obtained from basic material tests and evaluated based on the given dimensions of the cross-sectional area. Nevertheless, for the carbon-carbon bonds of CNTs, no classical tests or geometric derivations are available to describe the properties of the equivalent beam elements. Consequently, we assume the same values for the equivalent beam elements as in the approach proposed in [4, 20, 22]. These effective material and geometrical properties were obtained in the mentioned references based on a molecular mechanics approach where CNTs were regarded as a large molecule consisting of carbon atoms with atomic nuclei treated as material points. Their motions are regulated by a force field, which is generated by electron-nucleus interactions and nucleus-nucleus interactions, and usually expressed in the form of steric potential energy. This steric potential energy is in general the sum of contributions from bond stretch interaction, bond angle bending, dihedral angle torsion, improper (out of plane) torsion, and a non-bonded van der

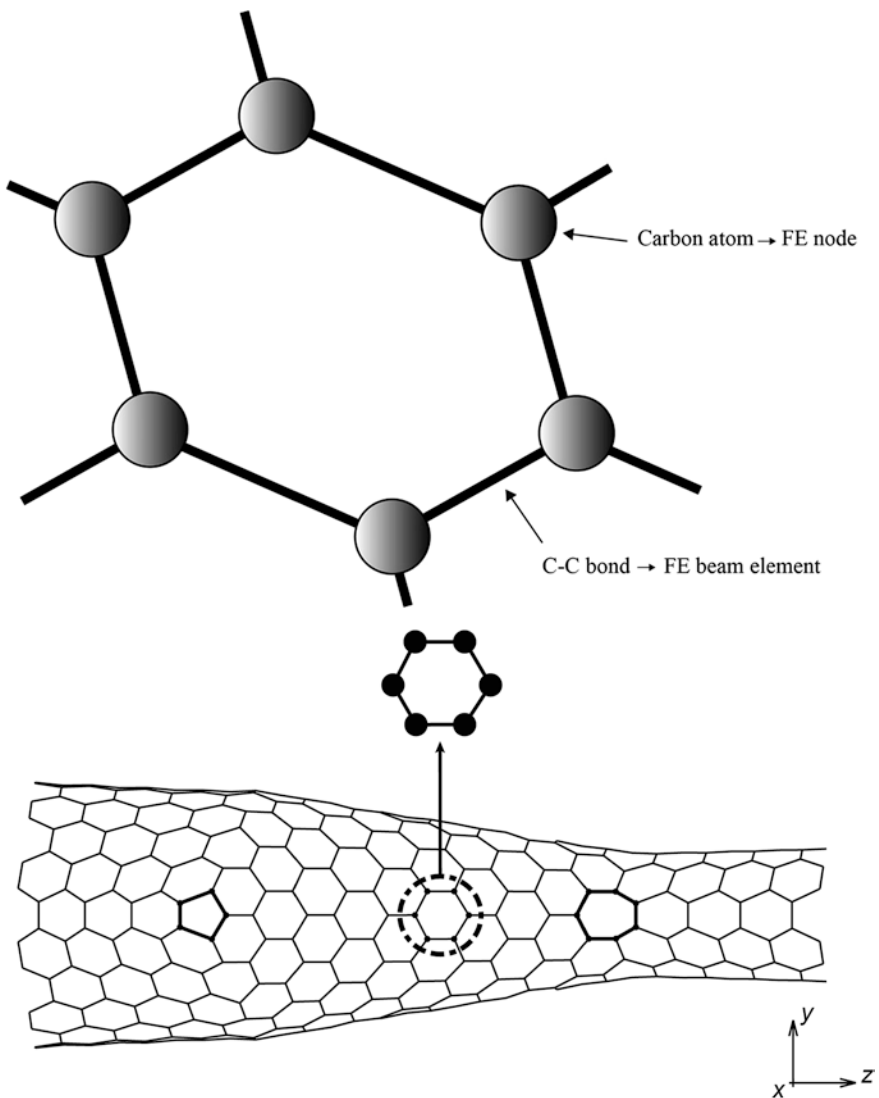


Fig. 7.1 Simulation of a hetero-junction CNT as a space-frame structure

Waals interaction in the case of multi-walled tubes, see Fig. 7.2. Li and Chou [20] applied the harmonic approximation and used further simplification to derive the energy expressions. These remaining energy expressions were equated with the corresponding energy expressions for a beam acquired from classical structural mechanics, as shown in Fig. 7.2. As a result, the stiffness parameters of the beam

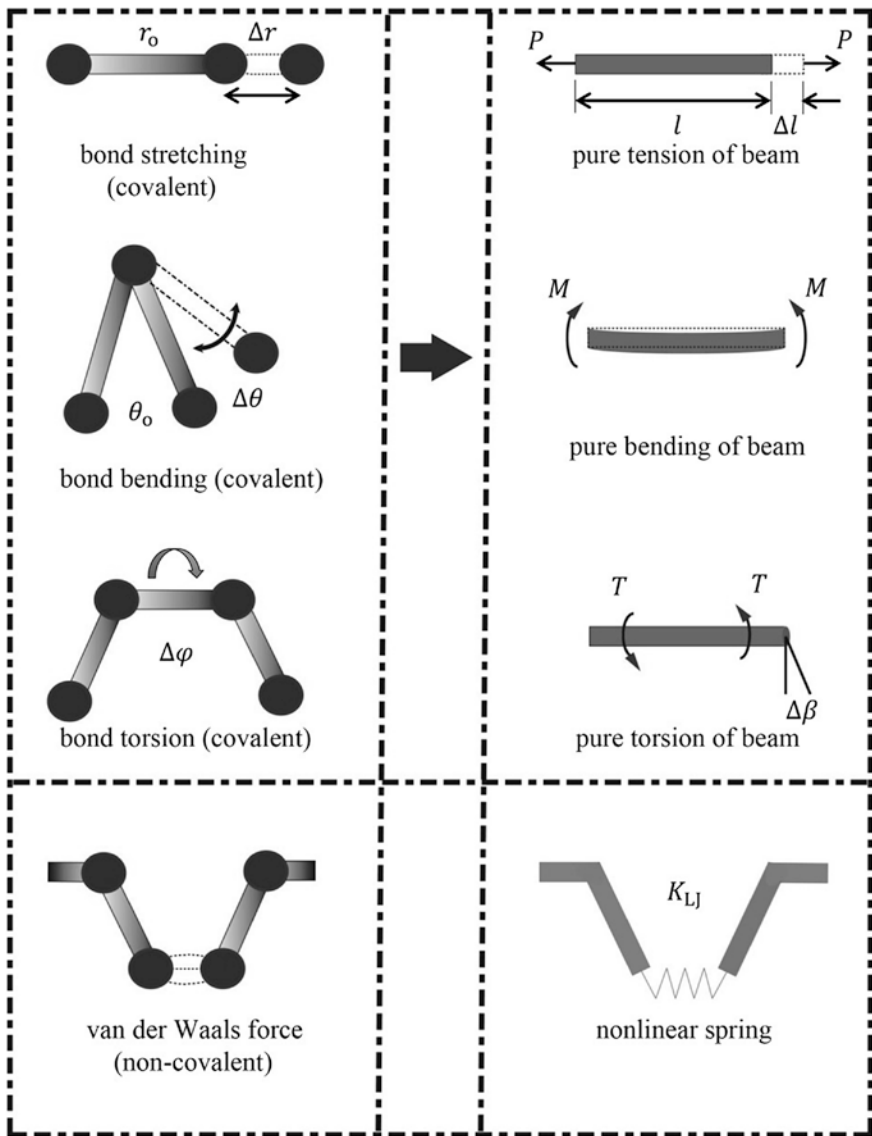


Fig. 7.2 Equivalence of molecular mechanics and structural mechanics for covalent and non-covalent interactions between carbon atoms. Molecular mechanics model (*left*) and structural mechanics model (*right*)

for elongation, bending and torsion were obtained as a function of three force field constants (available in literature) for stretching, bond angle bending and torsional resistance [48]. These introduced constants and the element properties are listed in Table 7.1.

Table 7.1 Material and geometric properties of C–C covalent bonds [68]

Corresponding force field constants	$k_r = 651.97 \text{ nN/nm}$
	$k_\theta = 0.8758 \text{ nN nm/rad}^2$
	$k_\varphi = 0.2780 \text{ nN nm/rad}^2$
$E = \text{Young's modulus} = \frac{k^2 b}{4\pi k_\theta}$	$5.484 \times 10^{-6} \text{ N/nm}^2$
$G = \text{shear modulus} = \frac{E}{2(v+1)}$	$2.159 \times 10^{-6} \text{ N/nm}^2$
$R_b = \text{bond radius} = 2\sqrt{\frac{k_\theta}{k_r}}$	0.0733 nm
$I_{xx} = I_{yy} = \text{second moments of area} = \frac{\pi R_b^4}{4}$	$2.2661 \times 10^{-5} \text{ nm}^4$

The weight of a SWCNT with a diameter d and a length l can be calculated from the surface area of a graphene sheet [69]:

$$W_{\text{SW}} = \frac{1}{1,315} \pi l d \text{ (g)} \quad (7.1)$$

For the case of MWCNTs with an inner diameter d_{int} , the same length l and a number of walls n , The surface area of all the graphene sheets which compose the MWCNT is [69]:

$$S_{\text{MW}} = \pi \cdot l \cdot \{d_{\text{int}} + (d_{\text{int}} + 2 \cdot d_{\text{s-s}}) + (d_{\text{int}} + 4 \cdot d_{\text{s-s}}) + \dots + [d_{\text{int}} + 2(n-1) \cdot d_{\text{s-s}}]\} \quad (7.2)$$

Where the inter-shell distance, $d_{\text{s-s}}$, is 0.34 nm. The above equation can be simplified as:

$$S_{\text{MW}} = \pi l \left[nd_{\text{int}} + 2d_{\text{s-s}} \sum_{i=0}^{n-1} i \right] \quad (7.3)$$

Each graphene sheet has a surface weight equal to 1/1315 g/m² and thus the weight of the MWCNT can be calculated:

$$W_{\text{MW}} = \frac{1}{1,315} \pi l \left[nd_{\text{int}} + 2d_{\text{s-s}} \sum_{i=0}^{n-1} i \right] \quad (7.4)$$

In order to simplify the comparison, taking the same length for the two CNTs, the weight of the MWCNT (W_{MW}) of inner diameter d_{int} (Eq. (7.4)) is divided by the weight of the SWCNT (Eq. (7.1)), 1 nm in diameter, giving the ratio R:

$$R = \frac{W_{\text{MW}}}{W_{(\text{SW}, 1 \text{ nm})}} = \left[nd_{\text{int}} + 2d_{\text{s-s}} \sum_{i=0}^{n-1} i \right] \quad (7.5)$$

The volume of one CNT depends on the outer diameter (d_{out}):

$$V_{\text{MW}} = \pi l d_{\text{out}}^2 / 4 \quad (7.6)$$

and the weight of the CNT is given by Eq. (7.4), transformed as a function of d_{out} as opposed to d_{int} :

$$W_{\text{MW}} = \frac{1}{1,315} \pi l \left[n d_{\text{out}} - 2 d_{\text{S-S}} \sum_{i=0}^{n-1} i \right] \quad (7.7)$$

The density of a MWCNT is thus [69]:

$$d_{\text{MW}} = 1,000 \cdot W_{\text{MW}} / V_{\text{MW}} \quad (7.8)$$

The theoretical maximum carbon wall density and mass density are closely related to the CNT diameters and for the case of MWCNTs, it is dependent to wall numbers [70]. In most of studies investigating the mechanical and physical properties of SWCNTs, the average value of mass density (ρ) of these nanostructures is 2.5 g/cm³ [71–73].

Chapter 8

Software Tools and Packages for Geometry Generation

8.1 CoNTub

A list of some common packages for simulating nanotubes is presented in Table 8.1.

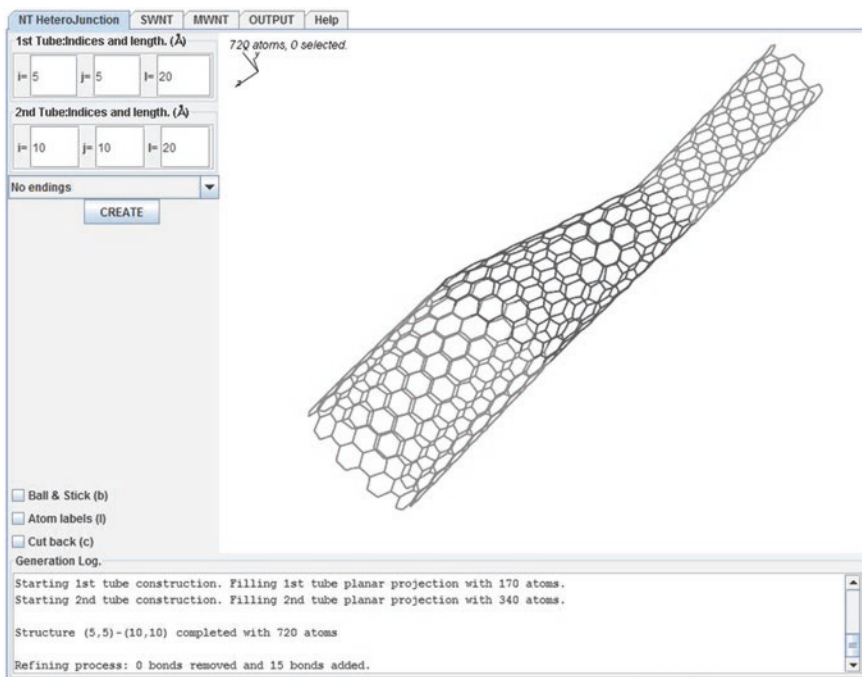
This software is used for modeling different types of CNTs. CoNTub is a computer program for determining the coordinates of these nanostructures. Defining the chirality and the length of the tubes, the spatial coordinates of the C-atoms and the corresponding connectivities (i.e. the primary bonds between two nearest-neighboring atoms) are calculated by this software. Some features of the first version of CoNTub are simulating SWCNTs and MWCNTs. The most highlighted feature of the second version of this software is to generate the models of three-junctioned CNTs. The Fig. 8.1 displays a snapshot from CoNTub software.

8.2 Carbon/Boron Nitride Nanostructure Builder Plugin

Using this plugin, models of carbon or boron nitride nanoparticles including single-wall nanotubes or graphene-like sheets can be simulated. The plugin itself only computes the carbon atom positions according to the provided input, but then has the option to generate further topology information suitable for classical force field MD simulations, which can then be stored in files of a suitable format. The nanotube builder plugin generates the unit cell of a SWCNT by first generating coordinates of a rectangular graphene sheet with dimensions corresponding to the particular chiral indices specified by the user. These coordinates are then mapped onto a cylinder to generate the SWCNT unit cell with its central axis aligned in the z-direction. The unit cell is then replicated along the longitudinal axis to generate a SWCNT of the desired length.

Table 8.1 Some common packages for geometry generation

Software	Corresponding web page
CoNTub	http://www.ugr.es/~gmdm/contub.htm
Carbon/Boron Nitride nanostructure builder plugin	http://www.ks.uiuc.edu/Research/vmd/plugins/nanotube/
Nanotube modeler	http://www.jcrystal.com/
TubeGen	http://turin.nss.udel.edu/research/tubegenonline.html
Ascalaph designer	http://www.biomolecularmodeling.com/Ascalaph/Ascalaph_Designer.html
Atomistix toolkit	http://quantumwise.com/
Materials Studio	http://accelrys.com/products/materials-studio/
Scigress	http://www.fqs.pl/chemistry_materials_life_science/products/scigress

**Fig. 8.1** The view of CoNTub software [74]

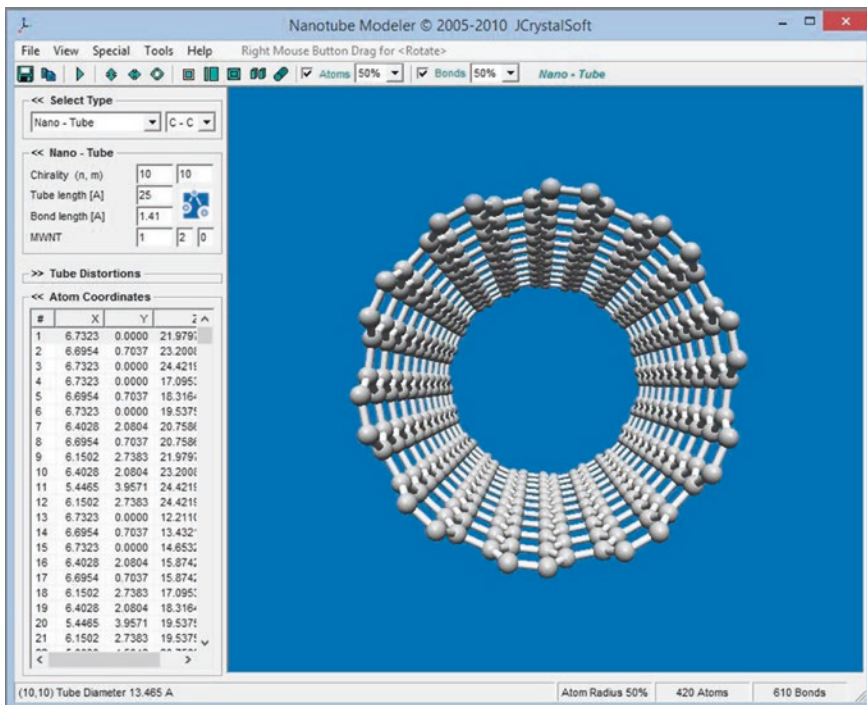


Fig. 8.2 The view of nanotube modeler [74]

8.3 Nanotube Modeler

This program is used for generating xyz-coordinates for nanotubes and nanocones. Nanotube modeler is based on the JNanotubeApplet but has improved and extended features. Some of the most important features of this software are modeling nanotubes, nanocones, buckyball, graphene sheets, nanotube hetero-junctions (using CoNTub plug-in), custom MWCNT input /radius calculator /MWCNT sequence finder. Figure 8.2 illustrates a snapshot of this software.

Figure 8.3 illustrates the generated table of nanotube modeler which shows the coordinates and connectivity.

8.4 TubeGen

This program is another package for determining the coordinates of the CNTs. It generates the hexagonal, cubic and unrolled crystal cells.

1	340							
2	3.8869	0.0000	0.0000	3.8869	0.0000	1.4100	1	3
3	3.6966	1.2011	2.1150	3.8869	0.0000	1.4100	2	3
4	3.6966	1.2011	2.1150	3.6966	1.2011	3.5250	2	4
5	3.6966	1.2011	2.1150	3.1445	2.2846	1.4100	2	27
6	3.8869	0.0000	1.4100	3.6966	-1.2011	2.1150	3	218
7	3.6966	1.2011	3.5250	3.8869	0.0000	4.2300	4	5
8	3.6966	1.2011	3.5250	3.1445	2.2846	4.2300	4	29
9	3.8869	0.0000	4.2300	3.8869	0.0000	5.6400	5	7
10	3.8869	0.0000	4.2300	3.6966	-1.2011	3.5250	5	220
11	3.6966	1.2011	6.3450	3.8869	0.0000	5.6400	6	7
12	3.6966	1.2011	6.3450	3.6966	1.2011	7.7550	6	8
13	3.6966	1.2011	6.3450	3.1445	2.2846	5.6400	6	31
14	3.8869	0.0000	5.6400	3.6966	-1.2011	6.3450	7	222
15	3.6966	1.2011	7.7550	3.8869	0.0000	8.4600	8	9
16	3.6966	1.2011	7.7550	3.1445	2.2846	8.4600	8	33
17	3.8869	0.0000	8.4600	3.8869	0.0000	9.8700	9	11
18	3.8869	0.0000	8.4600	3.6966	-1.2011	7.7550	9	224
19	3.6966	1.2011	10.5750	3.8869	0.0000	9.8700	10	11
20	3.6966	1.2011	10.5750	3.6966	1.2011	11.9850	10	12
21	3.6966	1.2011	10.5750	3.1445	2.2846	9.8700	10	35
22	3.8869	0.0000	9.8700	3.6966	-1.2011	10.5750	11	226
23	3.6966	1.2011	11.9850	3.8869	0.0000	12.6900	12	13
24	3.6966	1.2011	11.9850	3.1445	2.2846	12.6900	12	37
25	3.8869	0.0000	12.6900	3.8869	0.0000	14.1000	13	15
26	3.8869	0.0000	12.6900	3.6966	-1.2011	11.9850	13	228
27	3.6966	1.2011	14.8050	3.8869	0.0000	14.1000	14	15
28	3.6966	1.2011	14.8050	3.6966	1.2011	16.2150	14	16
29	3.6966	1.2011	14.8050	3.1445	2.2846	14.1000	14	39
30	3.8869	0.0000	14.1000	3.6966	-1.2011	14.8050	15	230
31	3.6966	1.2011	16.2150	3.8869	0.0000	16.9200	16	17
32	3.6966	1.2011	16.2150	3.1445	2.2846	16.9200	16	41
33	3.8869	0.0000	16.9200	3.8869	0.0000	18.3300	17	19
34	3.8869	0.0000	16.9200	3.6966	-1.2011	16.2150	17	232
35	3.6966	1.2011	19.0350	3.8869	0.0000	18.3300	18	19
36	3.6966	1.2011	19.0350	3.6966	1.2011	20.4450	18	20
37	3.6966	1.2011	19.0350	3.1445	2.2846	18.3300	18	43
38	3.8869	0.0000	18.3300	3.6966	-1.2011	19.0350	19	234
39	3.6966	1.2011	20.4450	3.8869	0.0000	21.1500	20	21
40	3.6966	1.2011	20.4450	3.1445	2.2846	21.1500	20	45
41	3.8869	0.0000	21.1500	3.8869	0.0000	22.5600	21	23

Fig. 8.3 The view of coordinates and connectivity generated by nanotube modeler

8.5 Ascalaph Designer

This software is a general-purpose program for molecular dynamics simulations.

8.6 Atomistix ToolKit

Atomistix ToolKit (ATK) is a software package that offers unique capabilities for simulating nanostructures on the atomic scale. Some of the features of this software are:

- NEGF simulations to study transport properties like I–V characteristics of nano-electronic devices
- Powerful combination of DFT, semi-empirical tight-binding, classical potentials in the same package

- Advanced graphical user interface for building complicated structures like interfaces and transport systems
 - Plugin-based platform which can interface with external codes Python scripting interface.

8.7 Materials Studio

This software package is used for modeling and simulations of materials. The widespread usage of this software in advanced research of various materials, such as nanotubes, ceramics and metals made this package a significant modeling program. Software components of this package are:

- Analytical and Crystallization: to investigate, predict, and modify crystal structure and crystal growth.
 - Quantum and Catalysis.

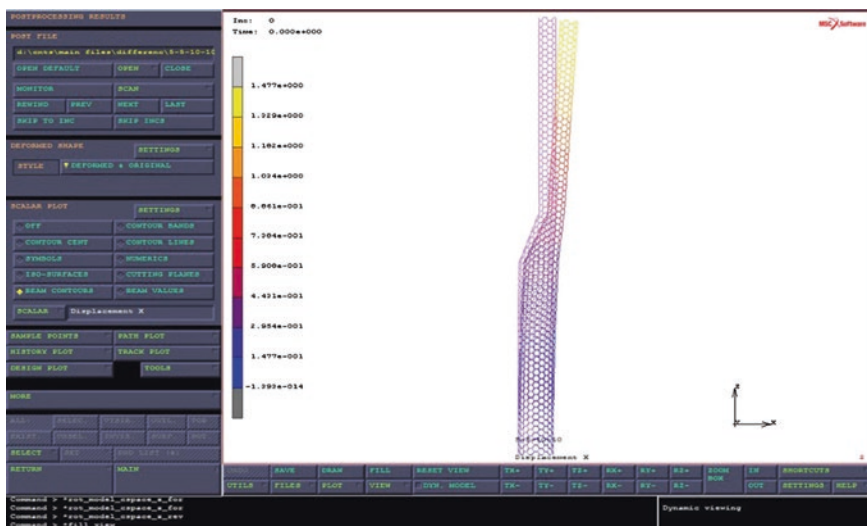


Fig. 8.4 The view of the result section of MSC. Marc software

Table 8.2 Some common FE programs

FE program	Corresponding web page
MSC Marc	http://www.mscsoftware.com/product/marc
Ansys	http://www.ansys.com/Products
Nastran	http://www.mscsoftware.com/product/msc-nastran
Abaqus	http://www.3ds.com/products-services/simulia/portfolio/abaqus/overview/

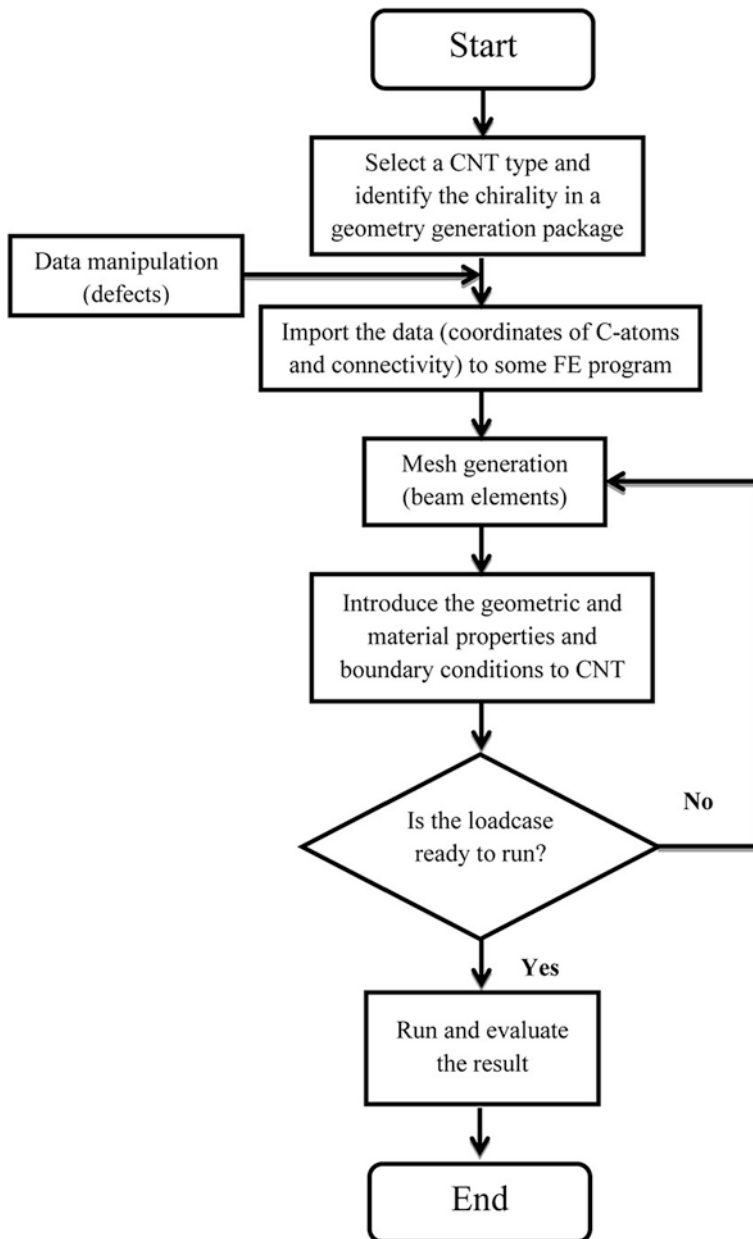


Fig. 8.5 Procedure of the simulation process, adopted from [75]

- Polymers and Classical Simulation: to construct and characterize models of isolated chains or bulk polymers and predict their properties.
- Materials Component Collection.
- Materials Visualizer.

8.8 Scigress

Sigress is a molecular modeling, computational chemistry and materials science software. It is used for chemistry and biochemistry. This package helps researchers to study and design a wide range of molecular systems.

After simulating the CNT models, the data will transfer to MSC Marc software so that the mechanical properties of different nanotubes could be obtained. The following figure illustrates the behavior of CNT under specific boundary condition (Fig. 8.4).

A list of some common FE program which can be used for simulations is presented in the Table 8.2.

The geometrical data of the CNTs is constructed by a package of geometry generation. Then the gathered data is transferred to a commercial finite element package (either directly or after a manipulation to consider different types of defects), where C–C bonds are modeled as circular beam elements. These elements are based on Timoshenko's beam theory with shear deformation effects included and the ability of torsional deformations around the longitudinal axis. This process is shown in the flowchart of Fig. 8.5.

References

1. Iijima S (1991) Helical microtubules of graphitic carbon. *Nature* 354:56–58
2. Iijima S, Ichihashi T (1993) Single-shell carbon nanotubes of 1-nm diameter. *Nature* 363:603–605
3. Bethune DS, Kiang CH, De Vries MS, Gorman G, Savoy R, Vazquez J, Beyers R (1993) Cobalt catalysed growth of carbon nanotubes with single-atomic-layer walls. *Nature* 363:605–607
4. To CWS (2006) Bending and shear moduli of single-walled carbon nanotubes. *Finite Elem Anal Des* 42:404–413
5. Mehdipour I, Barari A, Kimiaeifar A, Domairry G (2012) Vibrational analysis of curved single-walled carbon nanotube on a Pasternak elastic foundation. *Adv Eng Softw* 48:1–5
6. Yadav SK, Mahapatra SS, Cho JW, Park HC, Lee JY (2009) Enhanced mechanical and dielectric properties of poly(vinylidene fluoride)/polyurethane/multi-walled carbon nanotube nanocomposites. *Fiber Polym* 10:756–760
7. Natsuki T, Tantrakan K, Endo M (2004) Prediction of elastic properties for single-walled carbon nanotubes. *Carbon* 42:39–45
8. Liew KM, He XQ, Wong CH (2004) On the study of elastic and plastic properties of multi-walled carbon nanotubes under axial tension using molecular dynamics simulation. *Acta Mater* 52:2521–2527
9. Meo M, Rossi M (2006) Tensile failure prediction of single wall carbon nanotube. *Eng Fract Mech* 73:2589–2599
10. Tserpes KI, Papanikos P (2007) The effect of Stone-Wales defect on the tensile behavior and fracture of single-walled carbon nanotubes. *Compos Struct* 79:581–589
11. Xiao T, Ren Y, Liao K, Wu P, Li F, Cheng HM (2008) Determination of tensile strength distribution of nanotubes from testing of nanotube bundles. *Compos Sci Technol* 68:2937–2942
12. Kuang YD, He XQ (2009) Young's moduli of functionalized single-wall carbon nanotubes under tensile loading. *Compos Sci Technol* 69:169–175
13. Mohammadpour E, Awang M (2011) Predicting the nonlinear tensile behavior of carbon nanotubes using finite element simulation. *Appl Phys A* 104:609–614
14. Lu X, Hu Z (2012) Mechanical property evaluation of single-walled carbon nanotubes by finite element modeling. *Compos: Part B* 43:1902–1913
15. Ghavamian A, Rahmandoust M, Öchsner A (2012) A numerical evaluation of the influence of defects on the elastic modulus of single and multi-walled carbon nanotubes. *Comp Mater Sci* 62:110–116
16. Kinoshita Y, Murashima M, Kawachi M, Ohno N (2013) First-principles study of mechanical properties of one-dimensional carbon nanotube intramolecular junctions. *Comp Mater Sci* 70:1–7

17. Harris PJF (2004) Carbon nanotube composites. *Int Mater Rev* 49:31–43
18. Dreera S, Krismerb R, Wilhartitzc P, Friedbacher G (1999) Statistical evaluation of refractive index, growth rate, hardness and Young's modulus of aluminium oxynitride films. *Thin Solid Films* 354:43–49
19. Boubekera B, Taleaa M, Goudeaub PH, Coupeaub C, Grilheb J (2000) On the Young modulus of 304 L stainless steel thin films. *Mater Charact* 45:33–37
20. Li C, Chou TW (2003) A structural mechanics approach for the analysis of carbon nanotubes. *Int J Solids Struct* 40:2487–2499
21. Li C, Chou TW (2003) Elastic moduli of multi-walled carbon nanotubes and the effect of van der Waals forces. *Compos Sci Technol* 63:1517–1524
22. Kalamkarov AL, Georgiades AV, Rokkam SK, Veedu VP, Ghasemi-Nejad MN (2006) Analytical and numerical techniques to predict carbon nanotubes properties. *Int J Solids Struct* 43:6832–6854
23. Tsuda T, Ogasawara T, Deng F, Takeda N (2011) Direct measurements of interfacial shear strength of multi-walled carbon nanotube/PEEK composite using a nano-pullout method. *Compos Sci Technol* 71:1295–1300
24. Viet NV, Kuo WS (2012) Shear transfer in fractured carbon nanotubes under torsion. *Mater Sci Eng A* 536:256–264
25. Ghavamian A, Rahmandoust M, Öchsner A (2013) On the determination of the shear modulus of carbon nanotubes. *Compos: Part B* 44:52–59
26. Lui EM, Chen WF (1987) Steel frame analysis with flexible joints. *J Construct steel res* 8:161–202
27. Rahmandoust M, Öchsner A (2011) Buckling behaviour and natural frequency of Zigzag and Armchair single-walled carbon nanotubes. *J Nano Res* 16:153–160
28. Wang Y, Wang X, Ni X, Wu H (2005) Simulation of the elastic response and the buckling modes of single-walled carbon nanotubes. *Comp Mater Sci* 32:141–146
29. Kang Z, Li M, Tang Q (2010) Buckling behavior of carbon nanotube-based intramolecular junctions under compression: molecular dynamics simulation and finite element analysis. *Comp Mater Sci* 50:253–259
30. Mottevalli B, Montazeri A, Tavakoli-Darestani R, Rafii-Tabar H (2012) Modeling the buckling behavior of carbon nanotubes under simultaneous combination of compressive and torsional loads. *Physica E* 46:139–148
31. Poelma RH, Sadeghian H, Koh S, Zhang GO (2012) Effects of single vacancy defect position on the stability of carbon nanotubes. *Microelectron Reliab* 52:1279–1284
32. Ansari R, Rouhi S (2010) Atomistic finite element model for axial buckling and vibration analysis of single-layered graphene sheets. *Physica E* 43:58–69
33. Xin H, Han Q, Yao X (2007) Buckling and axially compressive properties of perfect and defective single-walled carbon nanotubes. *Carbon* 45:2486–2495
34. Talukdar K, Agrawala R, Mitra AK (2011) Dependence of mechanical characteristics and the fracture and buckling behavior of single-walled carbon nanotubes on their geometry. *New Carbon Mater* 26:408–416
35. Chang T, Li G, Guo X (2005) Elastic axial buckling of carbon nanotubes via a molecular mechanics model. *Carbon* 43:287–294
36. Arroyo M, Belytschko T (2005) Continuum mechanics modeling and simulation of carbon nanotubes. *Mecchanica* 40:455–469
37. Irvine T (1999) Application of the Newton-Raphson method to vibration problems. *Vibration data Publications*, Madison
38. Behera L, Chakraverty S (2013) Free vibration of Euler and Timoshenko nanobeams using boundary characteristic orthogonal polynomials. *Appl Nanosci* 4:347–358
39. Aydogdu M (2012) Axial vibration analysis of nanorods (carbon nanotubes) embedded in an elastic medium using nonlocal elasticity. *Mech Res Commun* 43:34–40
40. Ghavamian A, Öchsner A (2013) Numerical modeling of eigenmodes and eigenfrequencies of single- and multi-walled carbon nanotubes under the influence of atomic defects. *Comp Mater Sci* 72:42–48

41. Seyyed Fakhrabadi MM, Amini A, Rastgoo A (2012) Vibrational properties of two and three junctioned carbon nanotubes. *Comp Mater Sci* 65:411–425
42. Firouz-Abadi RD, Hosseiniyan AR (2012) Free vibrations of single-walled carbon nanotubes in the vicinity of a fully constrained graphene sheet. *Comp Mater Sci* 53:12–17
43. Biao K, Jianting D, Guanggui C, Xiuqin W, Zhen F, Zhiyong L (2010) Frequency shift of single walled carbon nanotube under axial load. *Int J Surf Eng* 4:503–504
44. Filiz S, Aydogdu M (2010) Axial vibration of carbon nanotube hetero-junctions using nonlocal elasticity. *Comp Mater Sci* 49:619–627
45. Ruoff RS, Yu MF (2005) Nanoscale mechanical characterization of carbon nanotubes. Microscale diagnostic techniques. In: Breuer KS (ed) Techniques, Springer series in electronics and electrical engineering. Chap. 5, pp 197–226
46. Dresselhaus MS, Dresselhaus G, Saito R (1995) Physics of carbon nanotubes. *Carbon* 33:883–891
47. Santiago P, Ascencio JA, Mendoza D, Perez-Alvarez M, Espinosa A, Reza-Sangerman C, Schabes-Retchkiman P, Camacho-Bragado GA, Jose-Yacaman M (2004) Synthesis and structural determination of twisted MoS₂ nanotubes. *Appl Phys A* 78:513–518
48. Rahmandoust M, Öchsner A (2012) On finite element modeling of single- and multi-walled carbon nanotubes. *J Nanosci Nanotech* 12:8129–8136
49. Dunlap BI (1994) Relating carbon tubules. *Phys Rev B* 49:5643–5650
50. Li M, Kang Z, Yang P, Meng X, Lu Y (2013) Molecular dynamics study on buckling of single-wall carbon nanotube-based intramolecular junctions and influence factors. *Comp Mater Sci* 67:390–396
51. Chico L, Crespi VH, Benedict LX, Louie SG, Cohen ML (1996) Pure carbon nanoscale devices: nanotube hetero-junctions. *Phys Rev Lett* 76:971–974
52. Imani Yengejeh S, Akbar Zadeh M, Öchsner A (2014) On the buckling behavior of connected carbon nanotubes with parallel longitudinal axes. *Appl Phys A* 115:1335–1344
53. Saito R, Fujita M, Dresselhaus G, Dresselhaus MS (1992) Electronic structure of chiral graphene tubules. *Appl Phys Lett* 60:2204–2206
54. Terrones M, Hsu WK, Hare JP, Kroto HW, Terrones H, Walton DRM (1996) Graphitic structures: from planar to spheres, toroids and helices. *Phil Trans R Soc A* 354:2025–2054
55. Iijima S, Ichihashi T, Ando Y (1992) Single-shell carbon nanotubes of 1-nm diameter. *Nature* 356:776–778
56. Meunier V, Henrard L, Lambin PH (1998) Energetics of bent carbon nanotubes. *Phys Rev B* 57:2586–2591
57. Saito R, Dresselhaus G, Dresselhaus MS (1996) Tunneling conductance of connected carbon nanotubes. *Phys Rev B* 53:2044–2050
58. Fejes D, Németh Z, Hernádi K (2009) CVD synthesis of spiral carbon nanotubes over asymmetric catalytic particles. *React Kinet Catal Lett* 96:397–404
59. Sugimoto Y, Shioya M, Matsumoto H, Minagawa M, Tanioka A (2013) Structure changes during tensile deformation and mechanical properties of a twisted carbon nanotube yarn. *Carbon* 60:193–201
60. Nath DCD, Sahajwalla V (2011) Application of fly ash as a catalyst for synthesis of carbon nanotube ribbons. *J Hazard Mater* 192:691–697
61. Li Y, Mi R, Li S, Liu X, Ren W, Liu H, Mei J, Lau WM (2014) Sulfur–nitrogen doped multi walled carbon nanotubes composite as a cathode material for lithium sulfur batteries. *Int J Hydrogen Energ* 39:16073–16080
62. Yuan N, Bai H, Ma Y, Ji Y (2014) First-principle simulations on silicon-doped armchair single-walled carbon nanotubes of various diameters. *Physica E* 64:195–203
63. Cheng Y, Tian Y, Fan X, Liu J, Yan C (2014) Boron doped multi-walled carbon nanotubes as catalysts for oxygen reduction reaction and oxygen evolution reaction in alkaline media. *Electrochim Acta* 143:291–296
64. Jaszcak JA, Robinson GW, Dimovski S, Gogotsi Y (2003) Naturally occurring graphite cones. *Carbon* 41:2085–2092

65. Lin CT, Lee CY, Chiu HT, Chin TS (2007) Graphene structure in carbon nanocones and nanodiscs. *Langmuir* 23:12806–12810
66. Lee JH, Lee BS (2012) Modal analysis of carbon nanotubes and nanocones using FEM. *Comp Mater Sci* 51:30–42
67. Brenner DW, Harrison JA, White CT, Colton RJ (1991) Molecular dynamics simulations of the nanometer-scale mechanical properties of compressed Buckminsterfullerene. *Thin Solid Films* 206:220–223
68. Lu JP (1997) Elastic properties of carbon nanotubes and nanoropes. *Phys Rev Lett* 79:1297–1300
69. Laurent C, Flahaut E, Peigney A (2010) The weight and density of carbon nanotubes versus the number of walls and diameter. *Carbon* 48:2994–2996
70. Chiadarelli N, Richard O, Bender H, Heyns M, De Gendt S, Groeseneken G, Vereecken PM (2012) Correlation between number of walls and diameter in multiwall carbon nanotubes grown by chemical vapor deposition. *Carbon* 50:1748–1752
71. Aydin M, Akins DL (2010) Calculated dependence of vibrational band frequencies of single-walled and double-walled carbon nanotubes on diameter. *Vib Spectrosc* 53:163–172
72. Narendar S (2012) Differential quadrature based nonlocal flapwise bending vibration analysis of rotating nanotube with consideration of transverse shear deformation and rotary inertia. *Appl Math Comput* 219:1232–1243
73. Mustapha KB, Zhong ZW (2010) Free transverse vibration of an axially loaded non-prismatic single-walled carbon nanotube embedded in a two-parameter elastic medium. *Comp Mater Sci* 50:742–751
74. Melchor S, Dobado JA (2004) CoNTub: an algorithm for connecting two arbitrary carbon nanotubes. *J Chem Inf Comp Sci* 44:1639–1646
75. Imani Yengejeh S, Kazemi SA, Öchsner A (2014) On the influence of atomic modifications on the structural stability of carbon nanotube hybrids: numerical investigation. *Int J Appl Mech.* doi:[10.1142/S175882511450077X](https://doi.org/10.1142/S175882511450077X)